Towards identification of essential structural elements of organoruthenium(II)-pyrithionato complexes for anticancer activity

Kladnik, Jerneja; Kljun, Jakob; Burmeister, Hilke; Ott, Ingo; Turel, Iztok; Romero-Canelón, Isolda

DOI:
10.1002/chem.201903109

Towards Identification of Essential Structural Elements of Organoruthenium(II)-Pyrithionato Complexes for Anticancer Activity

Jerneja Kladnik,[a] Jakob Kljun,[a] Hilke Burmeister,[b] Ingo Ott,[b] Isolda Romero-Canelón,[c] Iztok Turel*,[a]

[a] J. Kladnik, dr. J. Kljun, prof. dr. I. Turel
Faculty of Chemistry and Chemical Technology, University of Ljubljana, Večna pot 113, SI-1000 Ljubljana, Slovenia; Iztok.Turel@fkkt.uni-lj.si

[b] H. Burmeister, prof. dr. I. Ott
Institute of Medicinal and Pharmaceutical Chemistry, Technische Universität Braunschweig, 38106 Braunschweig, Germany

[c] dr. I. Romero-Canelón
School of Pharmacy, Institute of Clinical Sciences, University of Birmingham, Birmingham B15 2TT, U.K

ABSTRACT:

Organoruthenium(II) complex with pyrithione (2-mercaptopyridine-*N*-oxide) **1a** has previously been identified by our group as a compound with promising anticancer potential without cytotoxicity on non-cancerous cells. To expand rather scarce research on these kind of compounds an array of novel chlorido and pta (1,3,5-triaza-7-phosphaadamantane) organoruthenium(II) complexes with methyl-substituted pyrithiones has been prepared. After thorough aqueous stability investigation further elucidation of complexes' mechanisms on cellular level was performed. Minor structural alterations introduced to ruthenium-pyrithionato compounds resulted in fine-tuning of cytotoxicity. The best performing compounds **1b** and **2b** with chlorido or pta ligand bound to ruthenium, respectively, and methyl on 3-position of pyrithione scaffold were further investigated. Both compounds trigger early apoptosis, induce ROS generation, G1 arrest in A549 cancer cells and show no strong interaction with DNA. However, only **1b** does also inhibit thioredoxin reductase. Besides, wound healing assay and mitochondrial function evaluation reveal differences of both compounds at cellular level.

KEYWORDS

Cancer, complex, pyrithione, ruthenium, thioredoxin reductase.

INTRODUCTION

The serendipitous discovery of the anticancer activity of cisplatin [*cis*-[$PtCl_2(NH_3)_2$] in the 1960s[1] and its subsequent introduction to clinical use in cancer therapy in the next decade has led to increased interest in the development of new metallopharmaceuticals.[2] Despite the great efficacy of platinum-based oncotherapeutics, their application can be hindered due to severe side effects and development of the drug resistance. Therefore, the demand for a discovery of new drugs is urgent. Currently, a lot of hope is put in two anticancer ruthenium compounds KP-1339 (also named NKP-1339 or IT-139) and TLD-1433 (**Figure 1A** and **1B**), which have entered clinical trials and have shown encouraging outcomes.[3] Besides, ruthenium(II)-arene-pta (RAPTA) complexes, e.g. RAPTA-C (**Figure 1C**), have shown very promising *in vitro* and *in vivo* results[4] and many other ruthenium compounds are being explored at preclinical stage.[5] In recent decades a lot of research has been focused on the synthesis of new potential organoruthenium(II)-arene anticancer compounds with piano-stool conformation with various chelating ligands, especially *N*,*N*-, *N*,*O*-, and *O*,*O*-donors, that express interesting biological properties.[6] Also some organoruthenium(II)-arene complexes with *O*,*S*-ligands were synthesized, though to a lesser extent.[7]

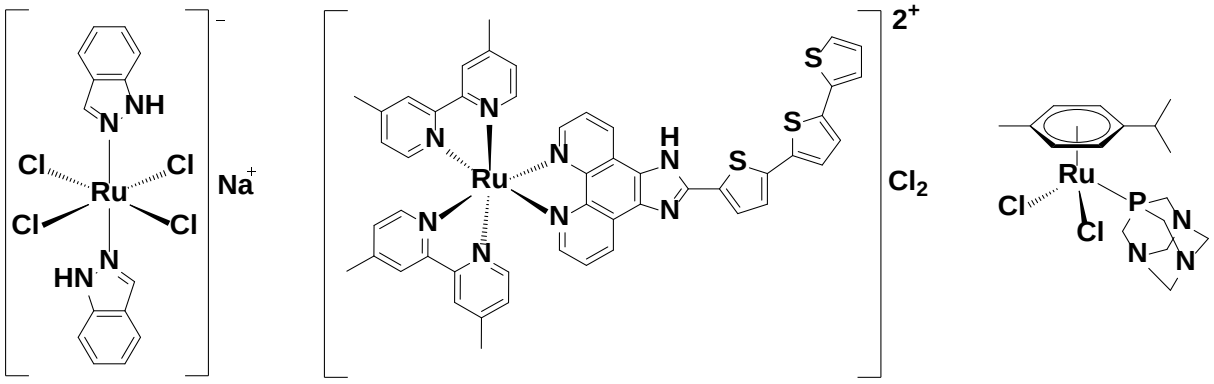

A: KP-1339 **B: TLD-1433** **C: RAPTA-C**

Figure 1: Examples of ruthenium-based therapeutics with prospective anticancer properties.

Pyrithione (**Figure 2**, **a**) is a cyclic thiohydroxamic acid,[8] which exists in solution in two tautomeric forms, preferably as 1-hydroxypyridine-2-thione as well as in minor share also as 2-mercaptopyridine-*N*-oxide.[9] In the solid state it adopts the thione form.[10] Pyrithione can bind to different metals *via O*- and *S*-atoms. Zinc pyrithione complex displays very good antimicrobial activity and is widely used as an active ingredient in commercial antidandruff shampoos and as a biocide in antifouling paints.[11] Further, iron, gallium and bismuth

pyrithione complexes are good antibacterial inhibitors against *Mycobacterium tuberculosis*,[12] platinum and palladium complexes show high antiparasitic activity on *Trypanosoma cruzi*,[13] vanadyl pyrithione possesses antidiabetic effects,[14] and nickel,[15] tin[16] and rhenium pyrithione complexes express anticancer properties.[17]

Recently, our research group was the first to report the synthesis of two η^6-*p*-cymene and two trithiacyclononane ruthenium(II) coordination compounds with pyrithione and its *O,O*-analogue, studying their anticancer activity. Interestingly, complexes with *O,O*-analogue induce the proliferation of the MCF-7 breast cancer cell line, whereas its *O,S*-analogue **1a** (**Figure 2**) shows a low EC_{50} value (3.81 ± 0.06 μM) along with potent inhibition of overexpressed aldo-keto reductase 1C enzymes (AKR1Cs).[18] Similar observations were noted in the case of hydroxy(thio)pyr(id)one complexes, where *O,S*-derivatives express better biological activity than parent hydroxypyr(id)ones, which is explained through lower stability of the oxygen-containing counterparts.[19] It was also reported previously by our group that complex **1a** was the only one among seventeen tested *N,N*-, *N,O*-, *O,O*- and *O,S*-organoruthenium(II) compounds, which displayed an inhibitory effect on glutathione-*S*-transferase (GST), the key enzyme involved in the development of the drug resistance in cancer treatment (IC_{50} = 2.26 ± 0.5 μM and IC_{50} = 45 ± 5.2 μM for GST from horse serum and human placenta, respectively). It was also proven that **1a** is not cytotoxic at pharmaceutically relevant concentrations against non-cancerous cell types, such as the HUVEC cell line and primary human keratinocytes (NHEK-1) cells. Moreover, while **1a** also possesses moderate inhibitory potency toward acetylcholinesterases and butyrylcholinesterase, target enzymes for treating Alzheimer's disease, it does not show any undesirable side effects whatsoever on the neuromuscular system at pharmacological concentrations.[20]

Complex **1a** with all the hitherto attractive anticancer characteristics thus represents our lead compound for further research. Therefore, the aim of this study was fine-tuning of physicochemical and biological properties by introducing minor structural changes to the lead compound **1a** to gain an insight which structural elements of complexes are important for anticancer activity and need to be taken into account when planning further lead compound optimisation. The synthesis of pyrithione **(Figure 2**, **a**) and its methyl-substituted analogues **b**–**e** (**Figure 2**) was first reported in 1950 and these sulphur analogues of antibiotic aspergillic acid have shown high *in vitro* antibacterial activity.[8] Cohen *et al.* have also shown that various methyl positions on pyrithione can have an enormous effect on the affinity in a metalloenzyme active site of human carbonic anhydrase II (hCAII).[21] The same group has

later prepared 21 more pyrithione analogues and further studied the structure-activity relationship of metal-binding pharmacophores.[22]

With these data in hand we have decided to prepare an array of ten organoruthenium(II) chlorido (**1a**–**e**) and pta (**2a**–**e**) complexes (**Figure 2**). After an in-depth study of their stability in biologically relevant conditions, all compounds were screened for the cytotoxicity on seven cancer cell lines for which IC_{50} values have been determined. The best-performing pair, namely **1b** and **2b**, was selected for further testing on one normal cell line and looking into their mode of action using assays such as wound healing assay, binding to bovine serum albumin (BSA), induction of apoptosis, cell cycle analysis, DNA interactions, generation of reactive oxygen species (ROS), inhibition of the potential molecular target thioredoxin reductase (TrxR) and mitochondrial function assay.

RESULTS AND DISCUSSION

Synthesis. Pyrithione analogues **b**–**e** were synthesized according to the reported procedure (**Figure S1**, Supplementary information)[21] and organoruthenium(II) chlorido (**1b**–**e**) and pta (**2a**–**e**) complexes were newly prepared in a two-step synthesis (**Figure 2**).

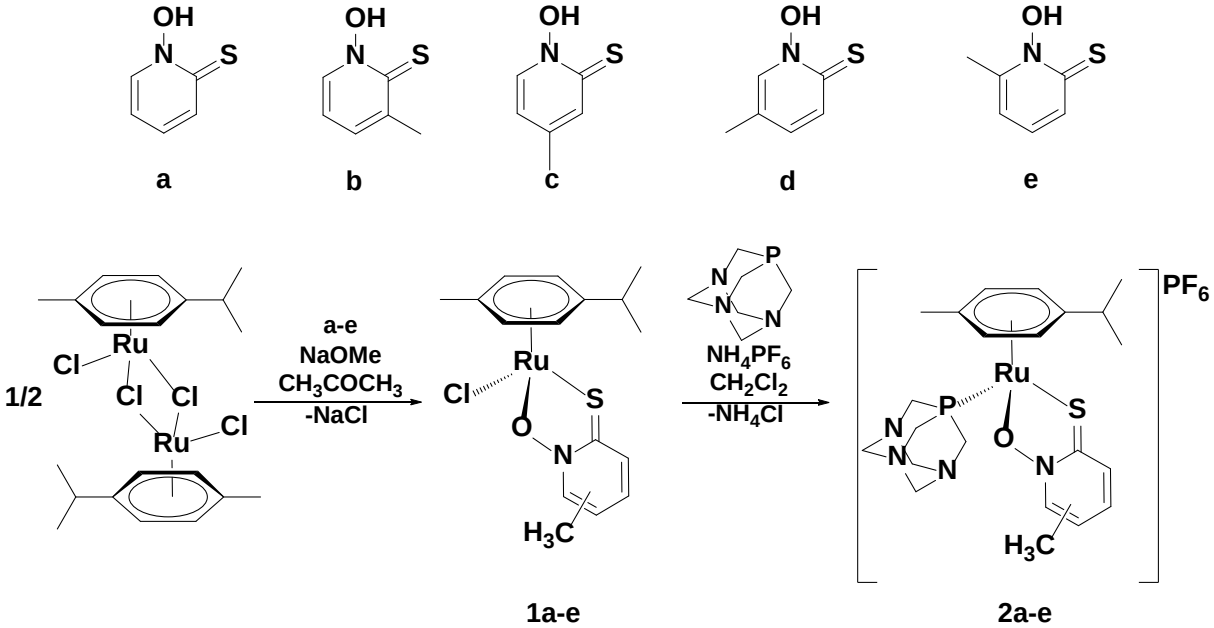

Figure 2: Scheme of prepared ligands and reaction path for organoruthenium(II) chlorido (**1a**–**e**) and pta (**2a**–**e**) complexes.

Neutral chlorido complexes **1a**–**e** were prepared with some modifications according to a previously reported procedure for **1a**.[18] The reaction mixture was stirred in acetone overnight

at room temperature. Sodium methoxide was used as a base to deprotonate the appropriate ligand and NaCl precipitated out as a byproduct. The deprotonation of the thiohydroxamic group enables the binding of the ligands via *S*- and *O*-atoms to the metal centre. Next day the solvent was evaporated and the chlorido complexes were purified by column chromatography on silica gel (mobile phase 5% DCM/acetone) to remove traces of unreacted ligands and precipitated NaCl. For the precipitation of all complexes a DCM/heptane solvent/antisolvent combination was used. After filtration under reduced pressure red solids were obtained, which are light, air, and moisture stable.

From the literature it is known that the organoruthenium(II) complexes with halides are prone to exchange their labile halido ligand with water as a first step of hydrolysis, form aqueous species and thus act as prodrugs.[23] In order to evaluate the importance and the effect of the aquation step on the mode of action and efficacy of the novel compounds we synthesized a second series of organoruthenium(II) complexes **2a**–**e**, in which the chlorido ligand from series **1** complexes was substituted with 1,3,5-triaza-7-phosphaadamantane (pta) neutral ligand. According to our research paper on organoruthenium(II)-diketonato complexes[24] and data from other research groups[25] the monodentate pta ligand is reported to slow down the hydrolysis rate and frequently increases the aqueous solubility of the complexes. Complexes **2a**–**e** were synthesized in dichloromethane (DCM) and stirred over two nights in the darkness to prevent decomposition. Chloride anion abstraction *via* NH_4PF_6 addition enables the binding of pta to ruthenium through the phosphorus atom, while NH_4Cl precipitates as a white salt. Importantly, to increase the yields pta needs to be ground in agate mortar to obtain a fine white powder as pta is only sparingly soluble in DCM. After the completion of the reaction, the reaction mixture was concentrated on rotary evaporator and precipitated NH_4Cl, unreacted NH_4PF_6 and pta were filtered off over Celite. The mother liquor was again partly evaporated and heptane was added to precipitate the product. However, during optimization cold diethyl ether proved to be a better antisolvent choice. The precipitates were left to stand in the fridge for around 10 minutes, followed by the filtration under reduced pressure after which yellow-orange solids were obtained. Although we have not noticed any visible changes after precipitation of pta complexes at ambient conditions, all pta complexes were stored in a desiccator protected from direct light exposure to prevent any possible decomposition reported previously for similar systems.[26]

Crystal structure determinations. Crystal structures were obtained for four ligands, three chlorido and five pta organoruthenium(II) complexes (**Figure 3**; **Figures S2–S4** and **Tables**

S1-S3, Supplementary information). Crystals for ligand **b**, **c, d** and **e** were achieved by solvent diffusion from DCM/*n*-heptane or DCM/*n*-hexane. The crystal structure for **1a** was already reported and crystalized from DCM/*n*-hexane mixture,[18] while the complexes **1b**, **1c** and **1e** crystalized using vapour diffusion method in solvent system chloroform/*n*-heptane. Compound **2a** and **2c** crystalized from DCM/*n*-hexane by solvent diffusion, whereas crystals for **2b**, **2d** and **2e** were obtained using the same solvent system but by vapour diffusion method. All compounds crystalized at ambient temperature, except from **2c** which crystallized at 4 °C.

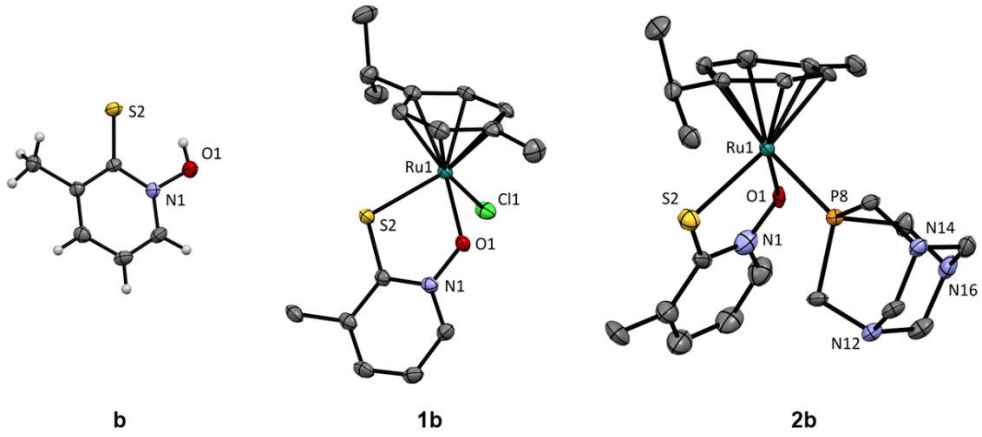

Figure 3: Crystal structures of selected compounds – ligand **b**, chlorido **1b** and pta **2b** complexes. The thermal ellipsoids are drawn at 35% probability level. In the structures of **1b** and **2b** hydrogen atoms are omitted for better clarity of presentation. In the structure of **2b** the PF_6^- anion is also omitted.

Crystal structures show that all ligands crystallize as the *N*-hydroxy-2-thione tautomers. The organoruthenium(II) complexes have pseudooctahedral geometry, where three coordination sites are occupied by the π-bound cymene ligand. The pyrithionato ligands are all bound in deprotonated form through the O1 and S2 atoms and the remaining site is occupied by the chlorido ligand in the series **1** compounds and by the phosphorous ligand pta in the series **2** compounds. The cationic structure of the series **2** compounds is counterbalanced by the hexafluorophosphate ion. Due to the minor nature of the structural modifications the bond distances and angles do not differ significantly from the previously reported parent structure.[18]

UV-Vis aqueous stability. Before conducting biological assays it is important to know how stable tested compounds are. Therefore, the stability of complexes was investigated by UV-Vis, ^{1}H and ^{31}P NMR spectroscopy at room temperature in different aqueous media. The conditions for these experiments aimed to mimic those used to perform cytotoxicity assays on

different cell lines. Hence, stock solutions of all complexes were prepared using 100% DMSO which were followed by the dilutions in biologically relevant matrixes to achieve working concentrations. The resulting working solution at 200 µM was in agreement with the highest concentration used for cell viability tests. Single beam UV-Vis scans were performed between 250 and 900 nm within 5 min of sample preparation and again after 24 h incubation at 37 ºC in the dark, using sealed cuvettes. The chosen matrixes included: water, phosphate-buffered saline (PBS), Roswell Park Memorial Institute 1640 cell culture medium (RPMI-1640), fully prepared RPMI-1640 which included the addition of 10% v/v fetal calf serum and 1% v/v pen/strep antibiotics and human blood plasma (UV-Vis spectra for **1b** and **2b** are presented in the Supplementary information, **Figures S5–S6**).

UV-Vis spectroscopy of metal-based complexes allows determination of changes in the metal coordination sphere by the observation of modifications in the UV-Vis trace. Hence, it is highly useful to establish complex stability in a given matrix using comparisons between two time point spectra. In particular, the relation between the results of water and PBS stability allows the detection of hydrolysis and its suppression by NaCl excess. Hydrolysis is often associated with metal-drug activation. In the case of the investigated chlorido and pta complexes, they all showed to be stable in these matrixes under the described conditions.

Similarly, investigations in RPMI-1640 and most importantly in fully prepared cell culture medium showed general complex stability which indicates that all chlorido and pta derivatives remain chemically unchanged under the conditions and in the timeframe used for biological activity experiments. Relevantly, this suggests that the complexes do not interact with the fetal calf serum included in the fully prepared cell culture medium. Such interaction could potentially alter the cellular accumulation of a given complex during cell-based assays. The final matrix to be investigated was human blood plasma, which is highly relevant when considering the development of a chemotherapeutic that would have an IV route of administration. All tested complexes resulted stable under the conditions described. It is worth highlighting that human plasma contains 140 mM chloride concentration and high albumin concentration, hence results in this matrix (taken together with results in PBS) are highly relevant. They suggest that the complexes would remain chemically stable when in systemic circulation and that any interactions with albumin do not include covalent binding to the metal centre, which may be beneficial for the transport and distribution of the drug. To further evaluate the interaction of complexes with bovine serum albumin (BSA), protein binding study was also conducted to confirm above stated results.

NMR aqueous stability. The stability of tested compounds was also investigated by ^{1}H and ^{31}P NMR spectroscopy to follow any possible structural changes. Spectra were recorded in 5% DMSO-d_6/D_2O and in 5% DMSO-d_6/D_2O containing 140 mM NaCl to evaluate the influence of the chloride, which is present at the same concentration in human plasma. Approximately 4 mg of **1b** or **2b** were first dissolved in DMSO-d_6 to facilitate dissolution and D_2O or D_2O containing NaCl was added to obtain 600 μL of 5% DMSO-d_6/D_2O solutions. Spectra were recorded immediately after the preparation and later at different time points. Complex **1b** turned out to be a very stable compound in both investigated media (**Figures S7–S8**, Supplementary information), which is in agreement with our previous report of stability for **1a**.[18] The first very small peaks of free *p*-cymene appear after one day at around 7.2 ppm and after twelve days at about 6.7 ppm. Chlorido complexes thus show favourable stability properties for the timeframes of conducted biological assays, which included 24 h drug exposure for IC_{50} determinations and 24 h or less for the determination of mechanism of action assays.

Further, the stability of complex **2b** was examined to evaluate the effect of the replacement of the chlorido ligand with pta (**Figures S9–S12**, Supplementary information). The initial changes in the NMR spectra in both media, though very small, appear after 3 hours in the aromatic region at around 7.2 ppm, when *p*-cymene starts dissociating from the ruthenium species. Furthermore, after 2 days additional small peak at around 6.7 ppm appears, also corresponding to free arene ring, which is consistent with the data of our organoruthenium(II) complexes with pta and *O,O*-ligands.[24] In 5% DMSO-d_6/D_2O small peaks appear after one day in the region between pta protons at around 4.4–4.0 ppm, which surprisingly correspond to the uncoordinated oxidized pta (ptao; 1,3,5-triaza-7-phosphaadamantane-7-oxide). Similar observation was also reported for RAPTA-type complexes with strongly electron-withdrawing arene ligands.[27] Also when the stability of **2b** was followed in 5% DMSO-d_6/D_2O containing NaCl another phosphorous species is present in minor share. Overall, when comparing the spectra less structural changes are observed in medium containing NaCl and considering these changes, NMR stability data are in good agreement with obtained UV-Vis results, which are both adequate for performing biological assays within appropriate timespan, as complexes are sufficiently stable in timeframe of biological experiments.

Cytotoxicity assay – determination of IC_{50} values. Ten organoruthenium(II) compounds were evaluated on seven different cell lines, including A549 lung, HCT116 colon, OE19 oesophageal, SKOV3 ovarian, HEPG2 hepatocellular, SW626 ovarian and PC3 prostate

cancer cells (**Table 1**). In general, complexes show good anticancer activity in low micromolar range in all tested cell lines. Remarkably, the best performance of complexes is observed in cell lines A549 and HCT116 of lung and colon origin, while the highest IC_{50} values are obtained in SW626 and PC3 lines of ovarian and prostate origin, with an approximate order of magnitude difference in potency between the former and the latter set of cell lines.

Table 1: Antiproliferative activity of prepared compounds on different cancer cell lines.

Compound	IC_{50} values (μM) on different cell lines[a]						
	A549	**HCT116**	**OE19**	**SKOV3**	**HEPG2**	**SW626**	**PC3**
1a	3.6 ± 0.3	14.1 ± 0.4	11.2 ± 0.3	7.5 ± 0.6	24.4 ± 0.4	27.8 ± 0.3	22.8 ± 0.3
2a	3.7 ± 0.3	13.7 ± 0.2	12.4 ± 0.3	9.2 ± 0.3	22.1 ± 0.9	30.4 ± 0.7	20.8 ± 0.2
1b	**1.86 ± 0.08**	**2.4 ± 0.3**	**4.0 ± 0.2**	**4.7 ± 0.3**	**8.3 ± 0.4**	**10.4 ± 0.7**	**12.8 ± 0.9**
2b	**2.21 ± 0.09**	**3.13 ± 0.08**	**3.95 ± 0.08**	**3.8 ± 0.7**	**7.9 ± 0.4**	**9.4 ± 0.2**	**10.5 ± 0.5**
1c	4.84 ± 0.07	*inactive*[b]	10.3 ± 0.5	14.6 ± 0.3	18.6 ± 0.7	32.6 ± 0.9	*inactive*[b]
2c	8.3 ± 0.4	*inactive*[b]	12.6 ± 0.7	*inactive*[b]	19.1 ± 0.8	21.2 ± 0.1	25.8 ± 0.6
1d	2.13 ± 0.09	6.3 ± 0.5	9.2 ± 0.3	6.8 ± 0.4	16.6 ± 0.5	19.3 ± 0.2	17.5 ± 0.9
2d	5.32 ± 0.06	5.4 ± 0.3	10.4 ± 0.6	7.5 ± 0.3	13.1 ± 0.6	22.6 ± 0.3	15.4 ± 0.6
1e	6.4 ± 0.2	10.5 ± 0.7	7.5 ± 0.3	12.6 ± 0.4	12.5 ± 0.6	15.3 ± 0.2	16.8 ± 0.3
2e	7.7 ± 0.2	8.8 ± 0.2	8.1 ± 0.4	13.5 ± 0.6	21.4 ± 0.3	16.1 ± 0.9	16.1 ± 0.7

[a]Values given are the mean IC_{50} values with standard deviations determined as duplicates of triplicates in two independent sets of experiments. Underlined are values, which show better activity of the complexes than our lead complexes **1a**/**2a**. [b]Compounds considered inactive have IC_{50} values above 150 μM under the following experimental conditions: 24 h drug exposure and 72 h recovery time in drug free medium, with 200 μM as the maximum concentration tested.

The comparison of the IC_{50} values of the complexes in a single cell line indicates that the included structural variations (i.e. position of methyl group) do alter their anticancer activity and we were able to establish preliminary structure activity relationship. By changing the position of single methyl substituent on the pyrithione scaffold anticancer activity of complexes on different cell lines is improved or diminished in comparison to our lead compound **1a**. Complexes **1b** and **2b** with a methyl group in the 3-position perform better in all tested cell lines (**Table 1**, underlined and bold values) compared to unsubstituted pyrithione complexes **1a** and **2a**. The same pattern was observed for **1d** and **2d** ruthenium complexes, except in one case (**2d** is less active in A549 cell line). Both ligands **b** and **d** bear methyl substituent on the positions, which donate electron density on sulphur and may like

that stabilize its binding to ruthenium centre. Still, **1b**-**2b** pair expresses higher anticancer activity in all cell lines as **1d**-**2d** pair. The activity of complexes on some cell lines is further reduced by changing methyl substituent on other positions. Remarkably, complexes **1c** and **2c** with a methyl substituent in the 4-position on pyrithione scaffold even resulted inactive on HCT116, SKOV3 and PC3 cells. Regarding chlorido substitution with pta ligand the IC_{50} values are comparable, though chlorido complexes do generally express better anticancer activity on A549, OE19, SKOV3 and SW626 and pta analogues on HCT116, HEPG2 and PC3 cell lines. This anticancer activity screening was conducted with an aim to obtain the clue where the structural changes in the later optimisation should be made. Gathered results do indicate that improved cytotoxicity can gradually be achieved by introducing small structural changes. In our case it turned out that by introducing methyl substituent on 3-position of pyrithionato scaffold makes complexes **1b** and **2b** the best performing compounds across all cell lines among all tested complexes and that electron-donor group needs to be placed on the position which increases electron density on sulphur. The activities of complexes **1b** and **2b** were the highest in A549 lung cancer and in view of these results, further investigations are focused on complexes **1b** and **2b** in A549 cell line in order to establish their mechanism of action on cellular level.

Cancer cell selectivity. Complexes **1b** and **2b** were further tested towards MRC5 lung fibroblasts (**Table 2**). Such experiment allows determination of selectivity factors, defined as the ratio between the IC_{50} values obtained in the normal cell line and the corresponding values in A549 cancer cells. This is an indication of the complexes' preferential toxicity towards cancer cells. Notably, both metal complexes are less toxic to MRC5 and have improved selectivity factor compared to one of cisplatin under similar experimental conditions.

Table 2: IC_{50} values of the selected compounds on A549 lung cancer and MRC5 normal cell lines and their selectivity factors.

Compound	**IC_{50} values (μM)**[a]		**Selectivity factor** [b]
	A549	**MRC5**	
1b	1.86 ± 0.08	8.75 ± 0.09	**4.70**[c]
2b	2.21± 0.09	9.1 ± 0.6	**4.11**[c]
Cisplatin	3.5 ± 0.2	11.5 ± 0.4	3.28

[a]Values given are the mean IC_{50} values with standard deviations determined as duplicates of triplicates in two independent sets of experiments. [b]Selectivity factors defined as the ratio between the IC_{50} value

in MRC5 normal fibroblasts divided by the corresponding value in A549 cancer cells. [c]Underlined are selectivity factors, which are better than the one of cisplatin.

Wound healing assay. We have explored how exposure to complexes **1b** and **2b** affects the migration of A549 cancer cells. During this assay, a gap or a wound is generated in a cellular monolayer and the rate of cell growth towards closing the gap is measured and compared between untreated controls and cells exposed to the metal complexes (**Figure S13 and Table S4**, Supplementary information). Untreated cells were able to close 75.1% of the gap within 24 h, while the complexes showed a concentration dependent effect on the wound recovery. Although at 2 µM the results of complex **1b** are comparable to the untreated controls (76.5%), at 4 µM the closing percentage is reduced to 44.7%, while for complex **2b**, the values are reduced to 30.4 and 19.2% at 2 µM and 4 µM, respectively. This assay is the first indication that small differences in the structure of both metal complexes could have a great effect on the cellular behaviour beyond their activity, expressed as IC_{50} values.

Protein binding studies. The so far described properties of the tested compounds have shown very favourable anticancer properties. However, the positive pharmacological effect of the drug is possible only if the compound reaches its target in a sufficient concentration. Albumin is the most abundant serum protein in the blood and can bind enormous numbers of drugs, thus acting also as a delivery system. Nonetheless, on the site of action only the unbound form of the drug could trigger pharmacological effects.[34] UV-Vis stability data of complexes in human plasma have shown very convenient results, which were additionally confirmed by a protein binding study, conducted for the complexes **1b** and **2b** on bovine serum albumin (BSA). Measurements were done at time point 0 and after 1 hour at a concentration of 3 µM of the complexes. Results have shown that at the beginning 81% (± 0.01) of the complex **1b** was bound to BSA and after one hour 71% (± 0.1) of complex remains bound to the protein. In case of **2b** at the beginning only a small quantity of the pta complex was bound to BSA (6% ± 0.1). However, after one hour the amount of bound **2b** increased to 58% (± 0.04). The higher reactivity of **1b** compared to **2b** is certainly related to the fact that the chlorido ligand of **1b** is a better leaving group than the pta ligand of **2b**. From obtained data we can conclude that albumin could act as one of the possible transporters for our complexes. Besides, compounds do also exist in their unbound form and can like that interact with therapeutic targets.

Induction of apoptosis. The induction of programmed cell death by complexes **1b** and **2b** has been investigated in A549 lung cancer cells after 24 h of drug exposure. This timeframe

has been set to coincide with the drug exposure time used for the determination of IC_{50} values. The flow cytometry analysis takes advantage of the cells that are double stained using Annexin V-FITC and propidium iodide. In a two-dimensional analysis cells that are single or double stained can be allocated into four subgroups: a) viable cells with low fluorescence in both flow cytometry channels, b) early apoptotic cells labelled only with Annexin after the loss of symmetry in the phospholipid membrane, c) late apoptotic cells that exhibit high fluorescence in both channels and d) non-viable cells that have become permeant to propidium iodide.

In these experiments untreated controls show a majority of the cellular population in the first a) subgroup (98%) (**Figure 4a; Table S5,** Supplementary information). By comparison, complexes **1b** and **2b** statistically increase the populations in the early apoptotic group b) in a concentration dependent manner. Remarkably, in any case there is no significant change in late apoptotic or non-viable cell population sets. This indicates that the cell death mechanisms, activated by the organoruthenium(II) complexes **1b** and **2b**, are triggered within the 24 h of drug exposure, but their final effects are only observed after the recovery time included in the experiments to determine IC_{50} values (72 h). This is consistent with light microscopy observation of A549 cells exposed to complexes **1b** and **2b,** which do not seem to show significant reductions in cell population after 24 h (**Figure S14**, Supplementary information). The observed induction of early apoptosis does not rule out the involvement of parallel mechanisms of cell death, in fact metal-based complexes which are frequently multi-targeted can often induce multiple mechanisms of action.

Cell cycle analysis. The influence of complexes **1b** and **2b** on the cell cycle of A549 lung cancer cells was further evaluated using flow cytometry and drug-exposed cells stained with propidium iodide (PI) after alcohol fixation. This experiment allows the detection of cellular populations in the G1, G2/M and S phase of the cell cycle. G1 and G2 are growth phases separated by S phase, when DNA is synthesized, and M phase, when mitosis occurs.[28] Cell cycle profiles are obtained by measuring PI fluorescence intensity in the FL2 red-channel as a reflection of quantitative DNA binding. The analysis used two concentrations of the organoruthenium(II) complexes and the results were compared against untreated controls. As expected, the negative controls showed the highest population percentage in G1 phase, followed by approximately equal populations in the G2/M and S phase (**Figure 4b; Table S6,** Supplementary information). Samples exposed to chlorido complex **1b** show a concentration dependent G1 arrest with its population increasing from 61% to 73 and 79%. Such G1 arrest

comes with the reduction of populations in the G2/M and S phases. Similar results were obtained for complex **2b** in which G1 populations increased to 70 and 72%. The lower arrest caused by the pta derivative **2b** could be correlated to the slightly reduced activity of this complex in comparison to the chlorido analogue. In both cases, a cellular arrest in the G1 phase highlights the potential cytostatic activity of both complexes as part of their multi-targeted mechanism of action and also indicates that they are less likely to rely on DNA-interactions as a part of their cellular anticancer behaviour. Such activity would be observed with a cell cycle arrest similar to cisplatin in S phase. This opens the possibility of exploiting the investigated complexes to overcome platinum resistance, which is a well-established clinical need. Compounds that bear metals other than platinum may have different mode of action and/or toxicity profile and can therefore offer new opportunities in combating resistance and/or side effects of platinum drugs.[29]

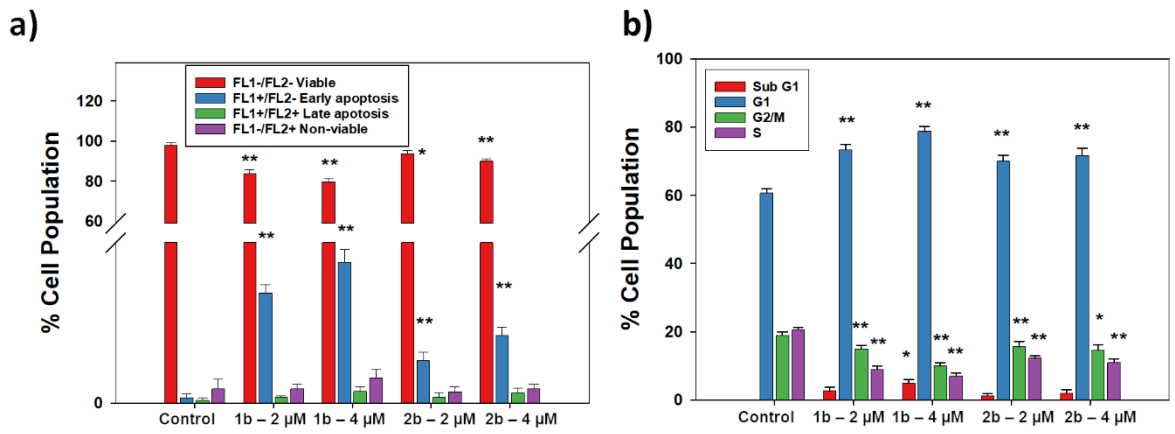

Figure 4: Flow cytometry investigations of A549 cancer cells exposed to complexes **1b** and **2b** for 24 h at 2 and 4 µM. Bar charts show the average percentage cell population present in each category in triplicate samples ($p<0.01$ for **, and $p<0.05$ for *). a) Induction of apoptosis and b) cell cycle analysis. Samples recorded reading Annexin V-FITC on FL-1 green channel and Propidium iodide on the FL-2 red channel and data processed using Flowjo.

DNA interactions. Given the results obtained in the cell cycle analysis of A549 cells exposed to complexes **1b** and **2b** we decided to confirm that the test-tube interactions of both complexes with Calf Thymus DNA (CT-DNA) were negligible. In a first experiment buffered solutions of CT-DNA and various concentrations of the metal complexes were incubated at 37 ^{o}C and re-evaluated after 24 h. Comparing the results obtained between 0 h and 24 h, together with comparisons against metal complex-only solutions, we were able to determine that there were no variations in the charge transfer bands for any of the complexes at any of the

concentration ratios measured (**Figures S15–16**, Supplementary information). A shift in wavelength or hypo/hyperchromism in such bands would be expected upon DNA-complex interaction. A second experiment included evaluation of the CT-DNA melting temperature in a buffered solution compared to samples that included a mixture of CT-DNA and the metal complexes. DNA melting point refers to the temperature, at which an equilibrium between single and double stranded DNA is established and perturbations of this value would indicate that the complexes are capable of disrupting or stabilising the DNA double helix. There were no changes in melting temperature detected, as both the CT-DNA and the mixtures of CT-DNA:complexes melted at approximately 66 °C (**Table S7**, Supplementary information). Such results are consistent with the previous observation that the cell cycles of A549 cells exposed to complexes **1b** and **2b** are not arrested in the S phase.

Induction of reactive oxygen species. Balanced redox state in the cell is crucial for maintaining diverse cellular functions[30] and organometallic complexes are often reported to be involved in the ROS generation in intracellular space.[31] Such activity may be well linked to their mode of action, particularly taking into account the high likelihood of metal complexes acting on multiple targets simultaneously.[30] Hence, ROS induction, initiated by exposure to compounds **1b** and **2b**, was investigated to see the effect of tested compounds in A549 lung cancer cells. These experiments included comparisons to known ROS inducers hydrogen peroxide and luperox. **Figure 5a** shows a statistically significant increase in the ROS induction of samples exposed to the complexes with concentration dependent trends. At each of the used concentrations, the increment of fluorescence intensity correlates to the increased potency and therefore to the cytotoxicity values determined, with complex **1b** generating most ROS followed by **2b** pta complexes (intensities 0.517 and 0.472, respectively). Such observations are consistent with a multi-targeted mechanism of action that involves modulation of the redox state of the cancer cells as higher cellular ROS concentrations may cause activation of different signalling pathways or damaging cellular components e.g. DNA, proteins, lipid components that leads to apoptosis of cells.[32] Interestingly, pyrithione zinc complex was also reported to increase ROS levels and induce death pathway in PC3 cell line.[33] On the other hand RAPTA-C and its analogues with *O*,*O*-diketonate ligands lack ROS production,[24] thus ROS generation in case of our pta **2b** complex probably derives from the ligand. Qualitative fluorescence microscopy results are in accordance with these quantitative results (**Figure 5b** and **5c**).

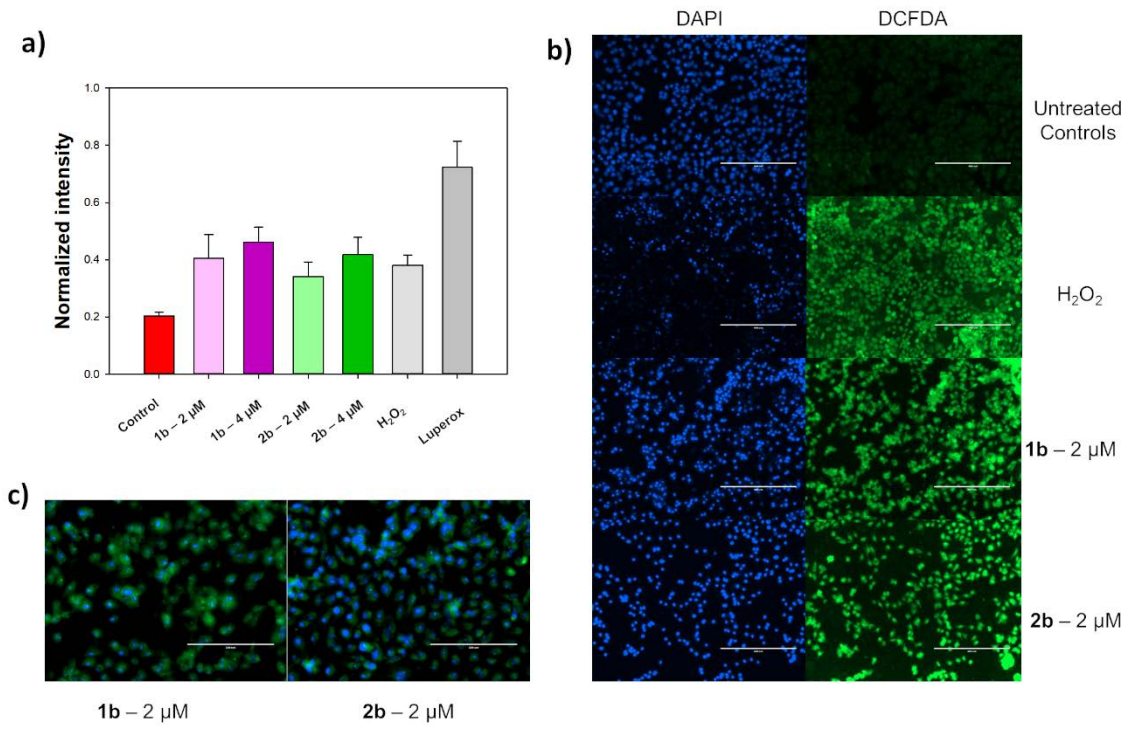

Figure 5: ROS induction on A549 cancer cells exposed to complexes **1b** and **2b** for 24 h at 2 and 4 µM: a) Bar chart shows quantitative measurements normalized to untreated controls, expressed as the mean ± standard deviations from triplicate samples, b) fluorescence microscopy unmerged channels using DAPI (blue) and DCFDA (green) with a 10x magnification and c) fluorescence microscopy using merged DAPI (blue) and DCFDA (green) channels with a 20x magnification.

Thioredoxin reductase inhibition. Considering cancer as one of the most complex diseases, the single-target drug approach seems to fail and it looks like that multi-target drugs now pave the way to achieve adequate therapeutic effects.[29, 35] Our lead compound **1a** has already shown good inhibition of AKR1C and glutathione-*S*-transferase, two enzymes involved in cancer progression.[18, 20] In literature arsenic complexes, including the one bearing a pyrithione ligand, have shown very good ability of inhibiting thioredoxin reductase (TrxR),[36] one of the crucial enzymes that regulates redox homeostasis in cells. If overexpressed, it can also cause cancer progression and the latter thus represents an interesting "druggable" target.[37] The first report on the significant TrxR inhibition of ruthenium(III) complexes was in 2007,[38] which triggered further studies with organoruthenium(II) compounds.[39-42] Hence, we have decided to conduct preliminary test of the inhibitory potency of **1b** and **2b** on TrxR, following an established protocol.[39, 40] Chlorido complex **1b** suppresses 45% of enzyme activity at tested 10 µM concentration compared to a positive control (enzyme not treated with compound), whereas pta complex **2b** show no inhibition on TrxR. From the literature it is known that metal compounds can promote cell death of cancer cells through ROS-mediated

apoptosis by targeting TrxR because the inhibition of TrxR induces accumulation of ROS.[43] Additionally, some Au-, Pt-, Cr-, Hg, As- and Se-compounds with anticancer activity express inhibition of TrxR, which resulted in DNA damage, elevated ROS levels and cell cycle changes that lead to apoptosis.[37] Both, higher generation of ROS as well as higher G1 arrest are observed for **1b** complex, which could be partly correlated with its TrxR inhibition. On the other hand, higher ROS generation and higher G1 arrest for **2b**, which do not inhibit TrxR, were also observed, but in lower extent and probably arise from other underlying mechanisms. It was also reported that some neutral Ru(II)-arene pta complexes are modest inhibitors of TrxR, whereas positively charged pta complexes, like in our case **2b**, trigger no relevant inhibition.[41] Some organoruthenium(II) complexes with *N*-heterocyclic carbene (NHC) ligands and labile halide also reduce activity of TrxR, but not the NHC ligands themselves.[39, 40, 44] We were also interested from where the inhibition of TrxR of our ruthenium complex **1b** is derived. Therefore, we have tested, whether only ligand **b** also influences TrxR activity. No inhibition of this enzyme by ligand **b** was detected. Obviously, the binding of pyrithione-based ligand to the metal centre proved to be essential for the inhibition of TrxR. Additionally, also halide ligand must be present for such activity of our organoruthenium(II) complexes. Although complex **1b** does not cause very strong inhibition of the enzyme, these results indicate that TrxR inhibition might be one of several factors that determine the cytotoxicity of the complex. In view of drug development identification of targets for biologically active compounds are crucial for understanding underlying mode of actions of the active compounds and for their further optimisation. Therefore, more studies to support these findings and to better understand the mechanism of action and possible targets are planned.

Evaluation of mitochondrial function. Given the results from the ROS induction and the behaviour of complexes **1b** and **2b** against TrxR we decided to investigate the mitochondrial function of A549 cells exposed for 24 h to the metal complexes. Therefore, we stained exposed cells with three fluorescent probes: DAPI, PI and Rhodamine-123 (Rh-123). The first probe enables sample and nuclei localisation, while PI acts as a marker for cell membrane integrity and the fluorescence of Rh-123 is indicative of mitochondrial function. The results shown in **Figure 6** confirm once more the differences at cellular level between complexes **1b** and **2b**. The former, which inhibits TrxR, reduces mitochondrial function in a concentration dependent manner and compromises cellular membrane only at high potency, while the later causes membrane damage and minimises mitochondrial function at both concentrations

tested. **Figure 6** also shows that the untreated controls do not have red fluorescence (from PI) and exhibit high Rh-123 signal.

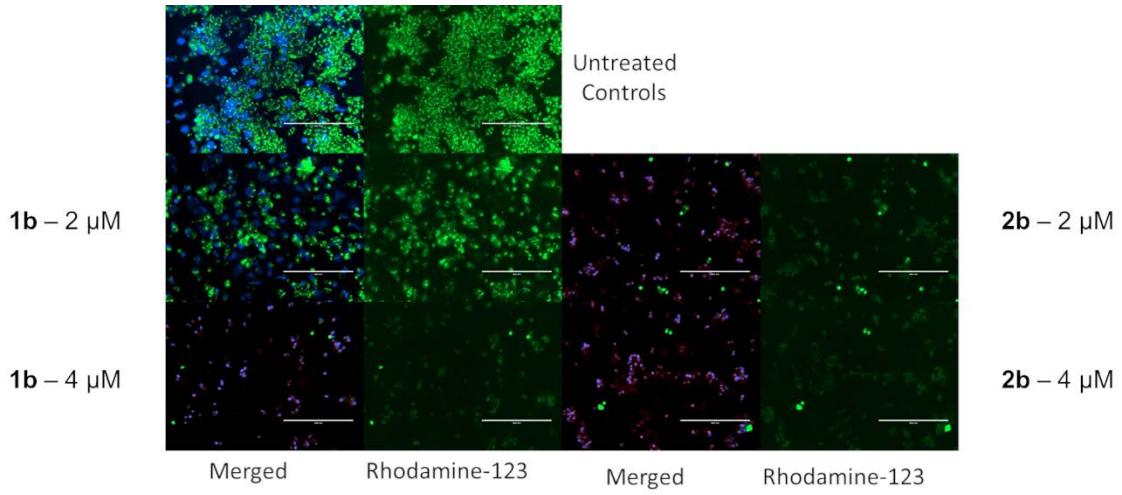

Figure 6: Evaluation of mitochondrial function on A549 cancer cells exposed to complexes **1b** and **2b** for 24 h at 2 and 4 μM. Fluorescence microscopy shows unmerged green channel using Rh-123 and merged images including DAPI (blue), propidium iodide (red) and Rh-123 (green), both with a 10x magnification.

CONCLUSIONS

A series of novel chlorido and pta organoruthenium(II) complexes with methyl-substituted pyrithiones have been prepared, fully characterized and examined for their anticancer properties. All compounds have shown sufficient stability in different aqueous media as well as in human blood plasma for further biological evaluation. Besides, protein binding study has additionally proven that albumin could act as a potential transporter of tested complexes. However, because of the reversible binding also free form of the compounds is available at the site of action. Compounds have shown to some extent comparable anticancer activities in very low micromolar range in cancer cell lines of different origin. Still, we were able to find some distinguishing patterns to establish preliminary structure-activity relationship. Importantly, complexes with ligand **b** and **d** bearing methyl substituent on positions, which increase electron density on sulphur, perform better than others. Generally, compounds express the lowest IC_{50} values on A549 lung cancer cells and among all cell lines compounds **1b** and **2b** have shown the best results. Determined cytotoxicity of the latter pair on normal cells has shown that the binding of the ligand to the metal centre increases selectivity toward cancer cell lines, with compound **1b** being at least toxic to normal cells. Further, most of the cell death mechanisms of complexes **1b** and **2b** are triggered within 24 h when early apoptotic

cells appear. Greater ROS generation as well as higher G1 arrest for **1b** and **2b** were also observed. Therefore, unlike cisplatin with its main target DNA causing S phase arrest, we suggest for our complexes multi-target mode of action. CT-DNA titrations and melting temperature experiments confirm no strong interactions between DNA and tested complexes, which is consistent with the results of cell cycle analysis causing G1 instead of S arrest. Higher percentage of cell population in early apoptotic group as well as in G1 phase of cell cycle and higher ROS generation of **1b** in comparison to **2b** seems to be mutually associated with TrxR inhibition which was observed for chlorido **1b** complex. It was also proven that ligand **b** itself cannot cause the inhibition of TrxR, whereas when bound to the ruthenium, it becomes active. Based on these results full anticancer potential of pyrithionato compounds is achieved only when appropriately substituted pyrithione ligand is bound to ruthenium metal centre together with halide ligand. Further, some discrepancies between chlorido and pta complexes, observed during the wound healing and mitochondrial function assays, point to different mechanisms of anticancer actions on cellular level. While chlorido complex **1b** shows concentration dependent wound recovery and reduced mitochondrial function, pta complex **2b** prevents closure of the wound as well as mitochondrial membrane damage at both concentrations tested. As the literature widely lacks new data in that specific area this study represents the first in-depth knowledge of organoruthenium(II)-pyrithionato compounds. Therefore, for future drug development these findings may aid to further rational design and should be taken into the consideration when planning new improved anticancer candidates of that type.

EXPERIMENTAL SECTION

Materials and methods. Ligand **a**, starting materials for the syntheses of ligands **b**–**e** and other reagents for the synthesis of complexes **1a**–**e** or **2a**–**e** were purchased from commercial suppliers (Fluorochem, Strem Chemicals) and used as received. Phosphine ligand pta was prepared according to the published procedure.[45] For the biological assays, propidium iodide (94%), RNAse, 2',7'–dichlorofluorescein diacetate (DCFH-DA), tert-butyl hydroperoxide (TBHP) and hydrogen peroxide were purchased from Sigma Aldrich. Solvents used for the reactions of the complexes were dried over sodium sulphate, whereas solvents used for the isolation of the compounds were used without further purification or drying. Pre-coated TLC sheets ALUGRAM® SIL G/UV_{254} (Macherey-Nagel) were used for following the progress of the reactions and were visualized under UV light. Column chromatography was performed

with Merck Silica gel 60 (35-70 μm) as a stationary phase. NMR spectroscopy was performed using Bruker Avance III 500 spectrometer at room temperature. ^{1}H NMR spectra were recorded at 500 MHz. Chemical shifts are referenced to deuterated solvent residual peaks $CDCl_3$, $(CD_3)_2CO$ or D_2O at 7.26 ppm, 2.05 ppm (referenced against the central line of quintet) or 4.79 ppm, respectively. ^{31}P spectra were recorded at 202 MHz and chemical shifts are reported relative to external standard. The splitting of proton resonances is defined as s = singlet, d = doublet, t = triplet, q = quartet, hept = heptet, m = multiplet, br = broad signal. Chemical shift (δ) and coupling constants (J) are given in ppm and Hz, respectively. All NMR data processing was carried out using MestReNova version 9.0.1 or 11.0.4. Infrared spectra were recorded with a Bruker FTIR Alpha Platinum ATR spectrometer. High resolution mass spectra (HRMS) were recorded on an Agilent 6224 Accurate Mass TOF LC/MS instrument. Elemental analyses were carried out on a Perkin-Elmer 2400 II instrument (CHN). UV-Vis spectra for compounds were collected on PerkinElmer LAMBDA 750 UV/Vis/near-IR spectrophotometer. UV-Vis stability measurements were carried out using a UV-Vis spectrophotometer UV-2600 Shimadzu. For the biological assays, 96-well plates were read using a FLUOStar Omega microplate reader, while flow cytometry analysis was done using Beckman Coulter Cytoflex and microscopy images were obtained with an EVOS PL system.

X-ray diffraction data was collected on an Oxford Diffraction SuperNova diffractometer with Mo/Cu microfocus X-ray source (Kα radiation, λ_{Mo} = 0.71073 Å, λ_{Cu} = 1.54184 Å) with mirror optics and an Atlas detector at 150(2) K. The structures were solved in Olex^2 graphical user interface[46] by direct methods implemented in SHELXT and refined by a full-matrix least-squares procedure based on F^2 using SHELXL.[47] All non-hydrogen atoms were refined anisotropically. The hydrogen atoms were placed at calculated positions and treated using appropriate riding models. The crystal structures have been submitted to the CCDC and have been allocated the deposition numbers 1912497-1912508 for compounds **b**–**e**, **1b**, **1c**, **1e** and **2a**–**e**, respectively.

Syntheses and characterization. Ligands **b**–**e** were prepared according to the known procedure,[21] with some modifications of *N*-oxidation according to another publication.[48] General scheme for the synthesis of ligands is provided in the Supplementary information (**Figure S1**). Chlorido and pta complexes were prepared with modifications of previously reported procedures from our group.[18, 24] The physico-chemical characterization of prepared compounds was performed by ^{1}H and ^{31}P NMR spectroscopy, infrared (IR), UV-Vis spectroscopy, CHN elemental analysis, high resolution electrospray ionization mass

spectrometry (ESI-HRMS) and for most of the compounds determined crystal structures have additionally confirmed all mentioned analyses. Purity of all synthesized compounds were confirmed by the use of NMR spectroscopy and CHN elemental analysis. Crystal structures, ^{1}H NMR and IR spectra are presented in the Supplementary information (**Figures S2–S4**, **S17–S34** and **S35–S44**, respectively).

General procedure b'–e' (*N*-oxidation). Appropriate 2-bromo-methylpyridine (1 mol. equiv.) was combined with *m*-chloroperoxybenzoic acid (*m*-CPBA, 2 mol. equiv., 70% purity) in DCM and stirred overnight at room temperature. The solution was first washed with 0.5 M $Na_2S_2O_{3(aq)}$ (W_1) and then with sat. $NaHCO_{3(aq)}$ (W_2). The organic phase was dried over sodium sulphate, filtered and evaporated under reduced pressure. The residue was purified by column chromatography on silica gel, eluting with 2% MeOH/DCM. After the removal of the solvent white solid or light yellow oil was obtained. Because of the partitioning of *N*-oxides in the organic and water phases further extractions of water phases W_1 and W_2 were needed. Water phase W_1 was extracted with DCM and the latter organic phase was washed with sat. $NaHCO_{3(aq)}$, which was further extracted with DCM. Water phase W_2 was extracted with DCM. The combined organic layers were dried over sodium sulphate, filtered and evaporated under reduced pressure.

*2-Bromo-3-methylpyridine-N-oxide (**b'**).* Yield: 72%. ^{1}H NMR (500 MHz, $CDCl_3$): δ = 8.29–8.25 (m, 1H, Ar–*H*), 7.15–7.07 (m, 2H, Ar–*H*), 2.46 (s, 3H, Ar–C*H*$_3$).

*2-Bromo-4-methylpyridine-N-oxide (**c'**).* Yield: 70%. ^{1}H NMR (500 MHz, $CDCl_3$): δ = 8.25 (d, 1H, *J* = 6.6 Hz, Ar–*H*), 7.47 (d, 1H, *J* = 2.1 Hz, Ar–*H*), 7.03 (dd, 1H, *J* = 6.6, 2.1 Hz, Ar–*H*), 2.33 (s, 3H, Ar–C*H*$_3$).

*2-Bromo-5-methylpyridine-N-oxide (**d'**).* Yield: 75%. ^{1}H NMR (500 MHz, $CDCl_3$): δ = 8.23 (s, 1H, Ar–*H*), 7.52 (d, 1H, *J* = 8.3 Hz, Ar–*H*), 6.95–6.92 (m, 1H, Ar–*H*), 2.29 (s, 3H, Ar–C*H*$_3$).

*2-Bromo-6-methylpyridine-N-oxide (**e'**).* Yield: 77%. ^{1}H NMR (500 MHz, $CDCl_3$): δ = 7.55 (dd, 1H, *J* = 8.0, 1.5 Hz, Ar–*H*), 7.23 (dd, 1H, *J* = 8.0, 1.5 Hz, Ar–*H*), 7.00 (t, 1H, *J* = 8.0 Hz, Ar–*H*), 2.58 (s, 3H, Ar–C*H*$_3$).

General procedure for b–e (thiolation). Appropriate 2-bromomethylpyridine-*N*-oxide **b'–e'** was dissolved in 1:1 (vol.) mixture of saturated $NaSH_{(aq)}$ and water (200 mg of substituted 2-bromopyridine-*N*-oxide per 20 mL of mixture) and left to stir at room temperature overnight.

The solution was acidified with 4 M $HCl_{(aq)}$ to pH = 1 and then immediately extracted with $CHCl_3$. The combined organic layers were dried over sodium sulphate, filtered and evaporated. The residue was triturated with acetone (approximately 3 mL), the byproduct elemental sulphur S_8 was filtered off and the mother liquor solution was evaporated to yield a yellow-greyish solid. Normally, so obtained compounds (based on NMR analysis purity over 95%) were used for further complexation with ruthenium precursor RuCym, as obtained thiones are sensitive to silica gel and partly decompose, which was similarly observed before.[49] Only if ligands were needed for any biological assays column chromatography on silica gel was carried out, eluting with hexane/ethyl acetate = 7/3, to afford yellow-greyish solid (yields given below before purification with column chromatography; yields after purification with column chromatography varied between 30–70% as already reported).[21]

*1-Hydroxy-3-methylpyridine-2(1H)-thione (**b**).* Yield: 80%, yellow solid. ^{1}H NMR (500 MHz, $CDCl_3$): δ = 12.47 (br s, 1H, N–O*H*), 8.05–8.02 (m, 1H, Ar–*H*), 7.31–7.28 (m, 1H, Ar–*H*), 6.70 (t, 1H, *J* = 7.1 Hz, Ar–*H*), 2.48 (s, 3H, Ar–C*H*$_3$). ESI-HRMS (CH_3CN) *m/z* for $[M + H]^+$ (found (calcd)): 142.0326 (142.0321). Anal. Calcd for C_6H_7NOS: C, 51.04; H, 5.00; N, 9.92. Found: C, 51.29; H, 4.79; N, 9.91.

*1-Hydroxy-4-methylpyridine-2(1H)-thione (**c**).* Yield: 91%, light yellow solid. ^{1}H NMR (500 MHz, $CDCl_3$): δ = 12.01 (br s, 1H, N–O*H*), 7.94 (d, 1H, *J* = 6.9 Hz, Ar–*H*), 7.51 (s, 1H, Ar–*H*), 6.59 (dd, 1H, *J* = 6.9, 2.2 Hz, Ar–*H*), 2.28 (s, 3H, Ar–C*H*$_3$). ESI-HRMS (CH_3CN) *m/z* for $[M + H]^+$ (found (calcd)): 142.0321 (142.0321). Anal. Calcd for C_6H_7NOS: C, 51.04; H, 5.00; N, 9.92. Found: C, 51.01; H, 4.66; N, 9.85.

*1-Hydroxy-5-methylpyridine-2(1H)-thione (**d**).* Yield: 85%, light yellow solid. ^{1}H NMR (500 MHz, $CDCl_3$): δ = 12.10 (br s, 1H, N–O*H*), 7.91 (s, 1H, Ar–*H*), 7.59 (d, 1H, *J* = 8.7 Hz, Ar–*H*), 7.13 (dd, 1H, *J* = 8.7, 1.7 Hz, Ar–*H*), 2.26 (s, 3H, Ar–C*H*$_3$). ESI-HRMS (CH_3CN) *m/z* for $[M + H]^+$ (found (calcd)): 142.0323 (142.0321). Anal. Calcd for C_6H_7NOS: C, 51.04; H, 5.00; N, 9.92. Found: C, 51.24; H, 4.86; N, 10.23.

*1-Hydroxy-6-methylpyridine-2(1H)-thione (**e**).* Yield: 85%, grayish solid. ^{1}H NMR (500 MHz, $CDCl_3$): δ = 12.59 (br s, 1H, N–O*H*), 7.56 (dd, 1H, *J* = 8.4, 1.0 Hz, Ar–*H*), 7.17 (dd, 1H, *J* = 8.4, 7.5 Hz, Ar–*H*), 6.61 (dd, 1H, *J* = 7.5, 1.0 Hz, Ar–*H*), 2.58 (s, 3H, Ar–C*H*$_3$). ESI-HRMS (CH_3CN) *m/z* for $[M + H]^+$ (found (calcd)): 142.0326 (142.0321). Anal. Calcd for C_6H_7NOS: C, 51.04; H, 5.00; N, 9.92. Found: C, 50.93; H, 5.01; N, 9.68.

General procedure for 1a–e. Reaction mixture, containing 90 mg of appropriate ligand **a–e** (2 mol. equiv.), precursor RuCym (1 mol. equiv.) and base NaOMe (1.9 mol. equiv.), was stirred overnight in acetone at room temperature. The solvent was removed under reduced pressure on a rotary evaporator and the crude product was purified by column chromatography on silica gel, eluting with 5% DCM/acetone. After combining the fractions, the mobile phase was evaporated under reduced pressure and an oily residue was obtained. To ensure total removal of methanol, the residue was dissolved in DCM (approximately 10 mL) and the solvent was again evaporated. The oily product was redissolved in 1–2 mL of DCM and addition of cold *n*-heptane (10–15 mL) resulted in the precipitation of the complex. If not, the solvents were partly evaporated on the rotary evaporator and the red solid precipitated out. Also ultrasonic bath was sometimes used to ease the precipitation. The suspension was left to stand for 15 minutes, then the product was filtered under reduced pressure and washed with cold *n*-heptane. Obtained red solid was left to dry overnight at 45 °C.

*[(η^6-p-Cymene)Ru(1-hydroxypyridine-2(1H)-thionato)Cl] (**1a**).* Yield: 57% (160 mg), red solid. ^{1}H NMR (500 MHz, $CDCl_3$): δ = 8.03 (dd, 1H, *J* = 6.8, 0.8 Hz, Ar–*H* a), 7.44 (dd, 1H, *J* = 8.3, 1.3 Hz, Ar–*H* a), 7.05–7.00 (m, 1H, Ar–*H* a), 6.71 (td, 1H, *J* = 6.8, 1.6 Hz, Ar–*H* a), 5.47 (d, 2H, *J* = 6.0 Hz, Ar–*H* cym), 5.27 (d, 2H, *J* = 6.0 Hz, Ar–*H* cym), 2.82 (hept, 1H, *J* = 6.9 Hz, Ar–C*H*$(CH_3)_2$ cym), 2.24 (s, 3H, Ar–CH_3 cym), 1.27 (d, 6H, *J* = 6.9 Hz, Ar–CH(CH_3)$_2$ cym). IR selected bands (cm^{-1}, ATR): 3034, 2964, 2870, 1544, 1453, 1172, 1131, 765, 708, 622. UV-Vis (λ (nm) (ε (L mol^{-1} cm^{-1})) *c* = 5 × 10^{-5} M, MeOH): 284 (10268), 490 (488). ESI-HRMS (CH_3CN) *m/z* for $[M - Cl]^+$ (found (calcd)): 362.0149 (362.0153). Anal. Calcd for $C_{15}H_{18}ClNORuS$: C, 45.39; H, 4.57; N, 3.53. Found: C, 45.13; H, 4.29; N, 3.50.

*[(η^6-p-Cymene)Ru(1-hydroxy-3-methylpyridine-2(1H)-thionato)Cl] (**1b**).* Yield: 52% (135 mg), red solid. ^{1}H NMR (500 MHz, $CDCl_3$): δ = 7.97 (dd, 1H, *J* = 6.8, 0.6 Hz, Ar–*H* b), 6.97 (dt, 1H, *J* = 7.1, 1.0 Hz, Ar–*H* b), 6.66 (t, 1H, *J* = 7.1 Hz, Ar–*H* b), 5.48 (d, 2H, *J* = 6.0 Hz, Ar–*H* cym), 5.27 (d, 2H, *J* = 6.0 Hz, Ar–*H* cym), 2.82 (hept, 1H, *J* = 7.0 Hz, Ar–C*H*$(CH_3)_2$ cym), 2.41 (s, 3H, Ar–CH_3 b), 2.24 (s, 3H, Ar–CH_3 cym), 1.26 (d, 6H, *J* = 7.0 Hz, Ar–CH(CH_3)$_2$ cym). IR selected bands (cm^{-1}, ATR): 3102, 2961, 2861, 1558, 1402, 1193, 1136, 1072, 777, 657. UV-Vis (λ (nm) (ε (L mol^{-1} cm^{-1})) *c* = 5 × 10^{-5} M, MeOH): 276 (12260), 488 (568). ESI-HRMS (CH_3CN) *m/z* for $[M - Cl]^+$ (found (calcd)): 376.0315 (376.0309). Anal. Calcd for $C_{16}H_{20}ClNORuS$: C, 46.77; H, 4.91; N, 3.41. Found: C, 46.45; H, 4.86; N, 3.30.

[(η^6-p-Cymene)Ru(1-hydroxy-4-methylpyridine-2(1H)-thionato)Cl] ***(1c)***. Yield: 57% (150 mg), red solid. ^{1}H NMR (500 MHz, $CDCl_3$): δ = 7.90 (d, 1H, J = 6.9 Hz, Ar–*H* c), 7.23 (d, 1H, J = 1.3 Hz, Ar–*H* c), 6.51 (dd, 1H, J = 6.9, 1.9 Hz, Ar–*H* c), 5.45 (d, 2H, J = 5.9 Hz, Ar–*H* cym), 5.25 (d, 2H, J = 5.9 Hz, Ar–*H* cym), 2.82 (hept, 1H, J = 7.0 Hz, Ar–C*H*$(CH_3)_2$ cym), 2.24 (s, 3H, Ar–C*H*$_3$ cym), 2.17 (s, 3H, Ar–C*H*$_3$ c), 1.27 (d, 6H, J = 7.0 Hz, Ar–CH(C*H*$_3)_2$ cym). IR selected bands (cm^{-1}, ATR): 3097, 2959, 2865, 1464, 1167, 1131, 856, 800, 775, 621. UV-Vis (λ (nm) (ε (L mol^{-1} cm^{-1})) c = 5 × 10^{-5} M, MeOH): 283 (12962), 489 (574). ESI-HRMS (CH_3CN) *m/z* for [M − Cl]$^+$ (found (calcd)): 376.0317 (376.0309). Anal. Calcd for $C_{16}H_{20}ClNORuS$: C, 46.77; H, 4.91; N, 3.41. Found: C, 46.73; H, 4.92; N, 3.45.

[(η^6-p-Cymene)Ru(1-hydroxy-5-methylpyridine-2(1H)-thionato)Cl] ***(1d)***. Yield: 52% (137 mg), red solid. ^{1}H NMR (500 MHz, $CDCl_3$): δ = 7.89 (s, 1H, Ar–*H* d), 7.32 (d, 1H, J = 8.4 Hz, Ar–*H* d), 6.87 (dd, 1H, J = 8.4, 1.1 Hz, Ar–*H* d), 5.46 (d, 2H, J = 6.1 Hz, Ar–*H* cym), 5.25 (d, 2H, J = 6.1 Hz, Ar–*H* cym), 2.82 (hept, 1H, J = 6.9 Hz, Ar–C*H*$(CH_3)_2$ cym), 2.24 (s, 3H, Ar–C*H*$_3$ cym), 2.14 (s, 3H, Ar–C*H*$_3$ d), 1.27 (d, 6H, J = 6.9 Hz, Ar–CH-(C*H*$_3)_2$ cym). IR selected bands (cm^{-1}, ATR): 3041, 2959, 2865, 1477, 1145, 850, 814, 744, 671, 542. UV-Vis (λ (nm) (ε (L mol^{-1} cm^{-1})) c = 5 × 10^{-5} M, MeOH): 281 (11358), 489 (518). ESI-HRMS (CH_3CN) *m/z* for [M − Cl]$^+$ (found (calcd)): 376.0315 (376.0309). Anal. Calcd for $C_{16}H_{20}ClNORuS$: C, 46.77; H, 4.91; N, 3.41. Found: C, 46.78; H, 4.81; N, 3.37.

[(η^6-p-Cymene)Ru(1-hydroxy-6-methylpyridine-2(1H)-thionato)Cl] ***(1e)***. Yield: 57% (149 mg), red solid. ^{1}H NMR (500 MHz, $CDCl_3$): δ = 7.31 (d, 1H, J = 8.1 Hz, Ar–*H* e), 6.91 (t, 1H, J = 7.6 Hz, Ar–*H* e), 6.61 (dd, 1H, J = 7.3, 0.7 Hz, Ar–*H* e), 5.50 (d, 2H, J = 4.4 Hz, Ar–*H* cym), 5.23 (s, 2H, Ar–*H* cym), 2.83 (hept, 1H, J = 7.0 Hz, Ar–C*H*$(CH_3)_2$ cym), 2.50 (s, 3H, Ar–C*H*$_3$ e), 2.24 (s, 3H, Ar–C*H*$_3$ cym), 1.31 (d, 6H, J = 7.0 Hz, Ar–CH(C*H*$_3)_2$ cym). IR selected bands (cm^{-1}, ATR): 3036, 2956, 2867, 1552, 1458, 1197, 1155, 863, 776, 651. UV-Vis (λ (nm) (ε (L mol^{-1} cm^{-1})) c = 5 × 10^{-5} M, MeOH): 279 (9832), 483 (510). ESI-HRMS (CH_3CN) *m/z* (found for [M − Cl]$^+$ (calcd)): 376.0310 (376.0309). Anal. Calcd for $C_{16}H_{20}ClNORuS$: C, 46.77; H, 4.91; N, 3.41. Found: C, 46.58; H, 4.79; N, 3.40.

General procedure for 2a–e. Reaction mixture, containing 80 mg of appropriate chlorido complex **1a–e** (1 mol. equiv.), ground phosphine ligand pta (1.5 mol. equiv.) and salt NH_4PF_6 (1.5 mol. equiv.), was stirred in dichloromethane (30 mL) in the darkness at room temperature over two nights during which the colour changed from red-orange to orange. The solvent was concentrated on rotary evaporator and the resulting suspension was filtered over a Celite pad

to remove precipitated NH_4Cl, unreacted NH_4PF_6 and pta. The mother liquor was concentrated (to approximately 2 mL) to obtain oily residue. Addition of cold diethyl ether (10–20 mL) resulted in the precipitation of the product. If needed ultrasonic bath was used to ease the precipitation. The suspension was left to stand for 10 min at 4 °C and the product was filtered and washed with diethyl ether. Yellow-orange solid was left to dry at 45 °C overnight.

[(η^6-p-Cymene)Ru(1-hydroxypyridine-2(1H)-thionato)pta]PF_6 ***(2a)****.* Yield: 74% (99 mg), light yellow solid. ^{1}H NMR (500 MHz, $(CD_3)_2CO$)): δ = 8.31 (dd, 1H, *J* = 6.9, 0.6 Hz, Ar–*H* a), 7.67 (dd, 1H, *J* = 8.3, 1.2 Hz, Ar–*H* a), 7.47–7.41 (m, 1H, Ar–*H* a), 7.14 (td, 1H, *J* = 6.9, 1.7 Hz, Ar–*H* a), 6.29 (d, 1H, *J* = 6.1 Hz, Ar–*H* cym), 6.19 (d, 1H, *J* = 6.1 Hz, Ar–*H* cym), 6.03 (d, 1H, *J* = 6.1, Ar–*H* cym), 5.87 (d, 1H, *J* = 6.1 Hz, Ar–*H* cym), 4.50 (s, 6H, *H* pta), 4.28–4.11 (m, 6H, *H* pta), 2.71 (hept, 1H, *J* = 7.0 Hz, Ar–C*H*$(CH_3)_2$ cym), 2.15 (s, 3H, Ar–C*H*$_3$ cym), 1.26 (dd, 6H, *J* = 15.2, 7.0 Hz, Ar–CH(C*H*$_3)_2$ cym). ^{31}P NMR (202 MHz, $(CD_3)_2CO$)): δ = –31.62 (*P*–pta), –144.25 (hept, J_{PF} = 708 Hz, *P*F_6). IR selected bands (cm^{-1}, ATR): 3112, 2932, 1460, 1242, 974, 947, 834, 765, 557, 481. UV-Vis (λ (nm) (ε (L mol^{-1} cm^{-1})) *c* = 5 × 10^{-5} M, MeOH): 297 (10986), 375 (2150). ESI-HRMS (CH_3CN) *m/z* for $[M - PF_6]^+$ (found (calcd)): 519.0924 (519.0921). Anal. Calcd for $C_{21}H_{30}F_6N_4OP_2RuS$: C, 38.01; H, 4.56; N, 8.44. Found: C, 37.89; H, 4.43; N, 8.29.

[(η^6-p-Cymene)Ru(1-hydroxy-3-methylpyridine-2(1H)-thionato)pta]PF_6 ***(2b)****.* Yield: 83% (110 mg), light yellow solid. ^{1}H NMR (500 MHz, $(CD_3)_2CO$)): δ = 8.20 (d, 1H, *J* = 6.7 Hz, Ar–*H* b), 7.39 (d, 1H, *J* = 7.1 Hz, Ar–*H* b), 7.07 (t, 1H, *J* = 7.1 Hz, Ar–*H* b), 6.28 (d, 1H, *J* = 6.1 Hz, Ar–*H* cym), 6.18 (d, 1H, *J* = 6.1 Hz, Ar–*H* cym), 6.03 (d, 1H, *J* = 6.1 Hz, Ar–*H* cym), 5.86 (d, 1H, *J* = 6.1 Hz, Ar–*H* cym), 4.48 (s, 6H, *H* pta), 4.26–4.08 (m, 6H, *H* pta), 2.73 (hept, 1H, *J* = 6.9 Hz, Ar–C*H*$(CH_3)_2$ cym), 2.48 (s, 3H, Ar–C*H*$_3$ b), 2.17 (s, 3H, Ar–C*H*$_3$ cym), 1.27 (dd, 6H, *J* = 16.2, 6.9 Hz, Ar–CH(C*H*$_3)_2$ cym). ^{31}P NMR (202 MHz, $(CD_3)_2CO$)): δ = –31.70 (*P*–pta), –144.25 (hept, J_{PF} = 707 Hz, *P*F_6). IR selected bands (cm^{-1}, ATR): 3087, 2964, 2875, 1427, 1240, 972, 946, 829, 581, 556. UV-Vis (λ (nm) (ε (L mol^{-1} cm^{-1})) *c* = 5 × 10^{-5} M, MeOH): 290 (12238), 369 (2782). ESI-HRMS (CH_3CN) *m/z* for $[M - PF_6]^+$ (found (calcd)): 533.1078 (533.1078). Anal. Calcd for $C_{22}H_{32}F_6N_4OP_2RuS$: C, 39.00; H, 4.76; N, 8.27. Found: C, 39.02; H, 4.72; N, 7.99.

[(η^6-p-Cymene)Ru(1-hydroxy-4-methylpyridine-2(1H)-thionato)pta]PF_6 ***(2c)****.* Yield: 80% (106 mg), dark orange solid. ^{1}H NMR (500 MHz, $(CD_3)_2CO$)): δ = 8.16 (d, 1H, *J* = 6.9 Hz, Ar–*H* c), 7.48 (s, 1H, Ar–*H* c), 6.97 (dd, 1H, *J* = 6.9, 2.1 Hz, Ar–*H* c), 6.26 (d, 1H, *J* = 6.1 Hz, Ar–*H* cym), 6.16 (d, 1H, *J* = 6.1 Hz, Ar–*H* cym), 6.01 (d, 1H, *J* = 6.1 Hz, Ar–*H* cym), 5.85 (d, 1H, *J*

= 6.1 Hz, Ar–*H* cym), 4.50 (s, 6H, *H* pta), 4.26–4.10 (m, 6H, *H* pta), 2.69 (hept, 1H, *J* = 6.9 Hz, Ar–C*H*$(CH_3)_2$ cym), 2.30 (s, 3H, Ar–C*H*$_3$ c), 2.14 (s, 3H, Ar–C*H*$_3$ cym), 1.25 (dd, 6H, *J* = 14.3, 6.9 Hz, Ar–CH(C*H*$_3$)$_2$ cym). ^{31}P NMR (202 MHz, $(CD_3)_2CO$)): δ = –31.58 (*P*–pta), –147.74 (hept, J_{PF} = 708 Hz, *P*F_6). IR selected bands (cm^{-1}, ATR): 2967, 2881, 1467, 1245, 974, 947, 832, 742, 581, 556. UV-Vis (λ (nm) (ε (L mol^{-1} cm^{-1})) *c* = 5 × 10^{-5} M, MeOH): 296 (11644), 379 (2062). ESI-HRMS (CH_3CN) *m/z* for $[M - PF_6]^+$ (found (calcd)): 533.1075 (533.1078). Anal. Calcd for $C_{22}H_{32}F_6N_4OP_2RuS$: C, 39.00; H, 4.76; N, 8.27. Found: C, 38.92; H, 4.74; N, 8.06.

[(η^6-p-Cymene)Ru(1-hydroxy-5-methylpyridine-2(1H)-thionato)pta]PF_6 ***(2d)***. Yield: 79% (105 mg), light yellow solid. ^{1}H NMR (500 MHz, $(CD_3)_2CO$)): δ = 8.18 (s, 1H, Ar–*H* d), 7.55 (d, 1H, *J* = 8.3 Hz Ar–*H* d), 7.33–7.29 (m, 1H, Ar–*H* d), 6.27 (d, 1H, *J* = 6.1 Hz, Ar–*H* cym), 6.17 (d, 1H, *J* = 6.1 Hz, Ar–*H* cym), 6.02 (d, 1H, *J* = 6.1, Ar–*H* cym), 5.84 (d, 1H, *J* = 6.1 Hz, Ar–*H* cym), 4.50 (s, 6H, *H* pta), 4.27–4.09 (m, 6H, *H* pta), 2.70 (hept, 1H, *J* = 7.0 Hz, Ar–C*H*$(CH_3)_2$ cym), 2.27 (s, 3H, Ar–C*H*$_3$ d), 2.14 (s, 3H, Ar–C*H*$_3$ cym), 1.25 (dd, 6H, *J* = 13.7, 7.0 Hz, Ar–CH(C*H*$_3$)$_2$ cym). ^{31}P NMR (202 MHz, $(CD_3)_2CO$)): δ = –31.67 (*P*–pta), –144.25 (hept, J_{PF} = 708 Hz, *P*F_6). IR selected bands (cm^{-1}, ATR): 2964, 2878, 1479, 1141, 972, 946, 833, 740, 576, 566. UV-Vis (λ (nm) (ε (L mol^{-1} cm^{-1})) *c* = 5 × 10^{-5} M, MeOH): 296 (11754), 379 (2192). ESI-HRMS (CH_3CN) *m/z* for $[M - PF_6]^+$ (found (calcd)): 533.1080 (533.1078). Anal. Calcd for $C_{22}H_{32}F_6N_4OP_2RuS$: C, 39.00; H, 4.76; N, 8.27. Found: C, 38.89; H, 4.76; N, 8.09.

[(η^6-p-Cymene)Ru(1-hydroxy-6-methylpyridine-2(1H)-thionato)pta]PF_6 ***(2e)***. Yield: 85% (112 mg), light orange solid. ^{1}H NMR (500 MHz, $(CD_3)_2CO$)): δ = 7.53 (dd, 1H, *J* = 8.3, 1.0 Hz, Ar–*H* e), 7.32 (t, 1H, *J* = 7.3 Hz, Ar–*H* e), 7.06 (dd, 1H, *J* = 7.3, 1.0 Hz, Ar–*H* e), 6.31 (d, 1H, *J* = 6.1 Hz, Ar–*H* cym), 6.22 (d, 1H, *J* = 6.1 Hz, Ar–*H* cym), 6.03 (d, 1H, *J* = 6.1 Hz, Ar–*H* cym), 5.85 (d, 1H, *J* = 6.1 Hz, Ar–*H* cym), 4.54–4.45 (m, 6H, *H* pta), 4.28–4.09 (m, 6H, *H* pta), 2.74 (hept, 1H, *J* = 6.9 Hz, Ar–C*H*$(CH_3)_2$ cym), 2.53 (s, 3H, Ar–C*H*$_3$ e), 2.17 (s, 3H, Ar–C*H*$_3$ cym), 1.29 (dd, 6H, *J* = 19.2, 6.9 Hz, Ar–CH(C*H*$_3$)$_2$ cym). ^{31}P NMR (202 MHz, $(CD_3)_2CO$)): δ = –31.28 (*P*–pta), –144.25 (hept, J_{PF} = 707 Hz, *P*F_6). IR selected bands (cm^{-1}, ATR): 3096, 2966, 2878, 1461, 1014, 974, 947, 834, 581, 557. UV-Vis (λ (nm) (ε (L mol^{-1} cm^{-1})) *c* = 5 × 10^{-5} M, MeOH): 289 (8670), 364 (2424). ESI-HRMS (CH_3CN) *m/z* for $[M - PF_6]^+$ (found (calcd)): 533.1075 (533.1078). Anal. Calcd for $C_{22}H_{32}F_6N_4OP_2RuS$: C, 39.00; H, 4.76; N, 8.27. Found: C, 38.96; H, 4.69; N, 8.27.

UV-Vis stability. 24 h stability was determined in biologically relevant matrixes including: a) water, b) PBS, c) RPMI-1640, d) fully prepared RPMI-1640 which included the addition of 10% v/v fetal calf serum and 1% v/v pen/strep antibiotics and e) human blood plasma. For these experiments, DMSO stock solutions of all complexes were prepared and further diluted in the corresponding matrixes. UV-Vis spectra were obtained twice (0 h and 24 h) between 250 and 900 nm using single beam scans with background correction. Samples were kept in sealed cuvettes at 37 °C between measurements.

Cell culture. All cell lines were obtained from the European Collection of Cell Cultures (ECACC). They were grown in Roswell Park Memorial Institute medium (RPMI-1640) supplemented with 10% fetal calf serum, 1% v/v 2 mM glutamine and 1% v/v penicillin/streptomycin (equivalent to 100 units/mL). Cells were grown as adherent monolayers in 25 or 75 cm^2 culture flasks at 37 °C in a 5% CO_2 humidified atmosphere and passaged at regular intervals, once 80% confluence was reached, using trypsin-EDTA.

Cytotoxicity assays, determination of IC_{50} values. Briefly, 5.000 cells were seeded per well in flat-bottom 96-well plates. The cells were pre-incubated in drug-free media at 37 °C for 48 h before adding different concentrations of the compounds to be tested. A stock solution of the compound was firstly prepared in 5% v/v DMSO and a mixture 0.9% saline and cell culture medium (1:1) (v/v) following serial dilutions in RPMI-1640 to achieve working solutions in which DMSO concentration did not exceed 0.5% v/v. The drug exposure period was 24 h. After this, supernatants were removed by suction and each well was washed with PBS. A further 72 h was allowed for the cells to recover in drug-free medium at 37 °C. The MTT assay was used to determine cell viability, with 4 h dye exposure in the dark. Absorbance measurements of the solubilized dye in DMSO allowed the determination of viable treated cells compared to untreated controls. IC_{50} values (concentrations which caused 50% of cell growth inhibition), were determined as duplicates of triplicates in two independent sets of experiments and their standard deviations were calculated.

Wound healing assay. A549 lung cancer cells were seeded in 24-well plates with 10.000 cells/well and allowed to reach 90% confluence. Following attachment, two “wounds” were created in each well using a pipette tip and cells were treated with complexes **1b** and **2b** using solutions as described above. After 24 h of drug exposure, drugs were removed by suction, cells were washed with PBS and stained using crystal violet solution prepared with 10% ethanol. Excess stain was washed with PBS and cells were visualised using a 4x transmission

microscope. A graph and numerical data can be found in the Supplementary information (**Figure S13** and **Table S4**).

Induction of apoptosis. The induction of cell death mechanism was investigated using flow cytometry and fluorescence microscopy using Annexin V-FITC and PI. For the former, A549 lung cancer cells were seeded in 6-well plates and allowed to attach for 24 h. Following attachment, cells were treated with complexes **1b** and **2b** using solutions as described above. After 24 h of drug exposure time, drugs were removed by suction, cells were washed with PBS and detached using trypsin. Single cell suspension were stained using PI/Annexin V-FITC in buffer. This experiment included negative untreated controls, and positive control cells induced with staurosporine (1 μg/mL). Cells for apoptosis studies were used with no previous fixing procedure as to avoid non-specific binding of the annexin V-FITC conjugate. These experiments were carried out in triplicates, full numerical data and statistical analysis can be found in the Supplementary information (**Table S5**). For the fluorescence microscopy experiments, cells were seeded using 8-well microscopy chambers with 5.000 cells/well. Drug treatment and staining was similarly carried out and readings were obtained using an EVOS FL microscope.

Cell cycle analysis. A million A549 lung carcinoma cells were seeded in 6-well plates. Cells are allowed to attach for 24 h in a 5% CO_2 incubator before adding various concentrations of complexes **1b** and **2b**. Drug solutions were prepared similarly to those used in the cytotoxicity assays in which DMSO concentration does not exceed 1%. Following 24 h of drug exposure, drugs were removed by suction, cells were washed with PBS and detached using Trypsin-EDTA. Single cell solutions were obtained and centrifuged to render cell pellets that were fixed for 2 h using ice-cold ethanol. Following fixation cell pellets were stained by re-suspending them in PBS containing propidium iodide (PI) and RNAse A. Samples were analysed by flow cytometry exploiting PI-bound DNA maximum excitation of at 536 nm, and its emission at 617 nm. Data were processed using Flowjo software. These experiments used untreated cells as negative controls. These experiments were carried out in triplicates, full numerical data and statistical analysis can be found in the Supplementary information (**Table S6**).

CT-DNA UV-Vis interactions. UV-Vis spectra investigations were performed to determine the DNA-binding affinity of complexes **1b** and **2b**. Experiments were carried out keeping fixed the concentration of the CT-DNA (75 μM) while varying the concentration the metal complexes (0, 5, 25, 50, 75, 100, 150 and 200 μM). The absorbance spectra were recorded

after 10 min of mixing each solution and again 24 h later. Graphs can be found in the Supplementary information (**Figures S15–16**).

CT-DNA melting. CT-DNA experiments were carried out in 10 mM phosphate buffer with 100 mM NaCl, at pH 7.5. In order to confirm that the CT-DNA was free from protein, a UV-VIS spectrum was carried out in the phosphate buffer, giving an absorbance ratio of 1.92:1 at 260 nm/280 nm. Its concentration was determined using the UV absorbance at 260 nm and the known extinction coefficient at this wavelength (6600 $dm^3mol^{-1}cm^{-1}$). Thermal denaturation of CT-DNA was recorded by measuring the absorbance at 260 nm while increasing the temperature between 50 °C and 95 °C. The melting curves of single CT-DNA or CT-DNA:complexes were recorded using a fixed ratio of 1:1 CT-DNA:complex (75 µM). The value of the melting temperature (T_m) as the temperature when 50% of the present double-stranded CT-DNA converts into single-stranded CT-DNA was determined as the corresponding maximum on the first-derivative profile of the melting curves. Numerical data can be found in the Supplementary information (**Table S7**).

Induction of reactive oxygen species (ROS). A549 lung carcinoma cells were seeded in 96-well black plates using 10.000 cells per well. Cells were allowed to attach for 24 h before adding increasing concentrations of complexes **1b** and **2b**. Working solutions used were obtained as described for the cytotoxicity assays. After 24 h of drug exposure, supernatants were removed by suction and the plates were washed with PBS. To each well, 100 µL of a 50 µM solution of 2',7'–dichlorofluorescein diacetate (DCFH-DA) were added and the plates were incubated with the dye in the dark for 2 h at 37 °C. Once cells were stained, supernatants were removed by suction and wells were washed with PBS before adding ROS inducers as positive controls. Hydrogen peroxide was used at 1 mM and tert-butyl hydroperoxide (TBHP) at 500 µM. ROS induction by positive controls was allowed for 2 h in the dark at 37 °C. Fluorescence readings were obtained with excitation at 485 nm and emission at 530 nm. This experiment included negative untreated controls, controls only treated with the metal complexes (to discard auto-fluorescence), untreated cells with hydrogen peroxide or TBHP, and complex treated cells with the ROS inducers.

Evaluation of mitochondrial function. A549 lung cancer cells were seeded in 8-well microscopy chambers with 5.000 cells/well and allowed to attach for 24 h. Following attachment, cells were treated with complexes **1b** and **2b** using solutions as described above. After 24 h of drug exposure time, drugs were removed by suction, cells were washed with

PBS, stained using DAPI/PI/Rh-123 in buffer and readings were obtained using an EVOS FL microscope. These experiments used untreated cells as negative controls.

Statistical analysis. In all cases, independent two-sample t-tests with unequal variances, Welch's tests, were carried out to establish statistical significance of the variations ($p<0.01$ for **, and $p<0.05$ for *).

Binding to albumin and inhibtion of TrxR. The experiments were performed as described in our previous reports.[40, 42, 50]

ACKNOWLEDGMENTS

We are grateful for financial support from the junior researcher grant for J. Kla. and the program Grant P1-0175 of the Slovenian Research Agency (ARRS). We thank the EN→FIST Centre of Excellence, Dunajska 156, SI-1000 Ljubljana, Slovenia, for the use of the SuperNova diffractometer. We would like to express our gratitude to dr. Katja Traven and dr. Matija Uršič for the help with obtaining crystallographic data and to Tjaša Rijavec and Meta Colnar for the help in the laboratory.

Supplementary information

General scheme for the synthesis of the ligands (**Figure S1**); Crystallographic data and structures for **b**–**e**, **1b**–**c**, **1e** and **2a**–**e** (**Tables S1–S3** and **Figures S2–S4**); Aqueous stability of **1b** and **2b** followed by UV-Vis Spectroscopy (**Figures S5–S6**); Aqueous stability of **1b** and **2b** followed by ^{1}H and ^{31}P NMR Spectroscopy (**Figures S7–S12**); The graph and numerical data for wound healing assay (**Figure S13**, **Table S4)**; Control data for induction of apoptosis in A549 cells (**Table S5)**; Light microscopy observations of A549 cells (**Figure S14**); Control data for the cell cycle analysis in A549 cells (**Table S6)**; Values of CT-DNA melting assay (**Table S7)**; UV-Vis spectra titrations of CT-DNA with complexes **1b** and **2b** (**Figures S15–S16)**; ^{1}H NMR spectra of **b'**–**e', b**–**e**, **1a**–**e** and **2a**–**e** (**Figures S17–S34**); IR spectra for **1a**–**e** and **2a**–**e** (**Figures S35–S44**).

AUTHOR CONTRIBUTIONS

Syntheses, characterization of the compounds and NMR stability were performed by J. Kla.. Crystal structures and crystallographic data were prepared by J. Klj.. UV-Vis stability, cytotoxicity assays, wound healing assay, induction of apoptosis, cell cycle analysis, CT-DNA UV-Vis titrations, CT-DNA melting, induction of ROS and evaluation of mitochondrial function were carried out by I.R.C.. Protein binding study was performed by H.B., TrxR inhibition was performed by J.Kla. and H.B.. I.O. helped with planning protein binding study and TrxR assay. J.Kla. wrote the manuscript with the help of I.R.C. who interpreted above mentioned biological assays and in consultations with J. Klj. and I.T.. I.T. coordinated and supervised the research and helped to shape the analyses and the manuscript. All authors provided critical corrections and have given approval to the final version of the manuscript.

ABBREVIATIONS

AKR1C, aldo-keto reductase 1C enzymes; BSA, bovine serum albumin; DCFH-DA, 2',7'–dichlorofluorescein diacetate; hCAII, human carbonic anhydrase II; IV, intravenous; NHC, *N*-heterocyclic carbene; PI, propidium iodide; pta, 1,3,5-triaza-7-phosphaadamantane; ptao, 1,3,5-triaza-7-phosphaadamantane-7-oxide; RAPTA, ruthenium(II)-arene-pta; RPMI-1640, Roswell Park Memorial Institute 1640 cell culture medium; RuCym, $[(\eta^6\text{-}p\text{-cymene})Ru(\mu\text{-}Cl)Cl_2]_2$; TrxR, thioredoxin reductase.

REFERENCES

[1] B. Rosenberg, L. Vancamp, J. E. Trosko and V. H. Mansour, *Nature* **1969**, *222*, 385-386.

[2] a) L. Kelland, *Nat. Rev. Cancer* **2007**, *7*, 573-584; b) I. Romero-Canelon and P. J. Sadler, *Proc. Natl. Acad. Sci. U.S.A.* **2015**, *112*, 4187-4188.

[3] a) H. A. Burris, S. Bakewell, J. C. Bendell, J. Infante, S. F. Jones, D. R. Spigel, G. J. Weiss, R. K. Ramanathan, A. Ogden and D. Von Hoff, *Esmo Open* **2016**, *1*; b) S. Thota, D. A. Rodrigues, D. C. Crans and E. J. Barreiro, *J. Med. Chem.* **2018**, *61*, 5805-5821; c) S. Monro, K. L. Colón, H. Yin, J. Roque, P. Konda, S. Gujar, R. P. Thummel, L. Lilge, C. G. Cameron and S. A. McFarland, *Chem. Rev.* **2019**, *119*, 797-828.

[4] a) C. Scolaro, A. Bergamo, L. Brescacin, R. Delfino, M. Cocchietto, G. Laurenczy, T. J. Geldbach, G. Sava and P. J. Dyson, *J. Med. Chem.* **2005**, *48*, 4161-4171; b) P. Nowak-Sliwinska, J. R. van Beijnum, A. Casini, A. A. Nazarov, G. Wagnieres, H. van den Bergh, P. J. Dyson and A. W. Griffioen, *J. Med. Chem.* **2011**, *54*, 3895-3902.

[5] L. Zeng, P. Gupta, Y. Chen, E. Wang, L. Ji, H. Chao and Z. S. Chen, *Chem. Soc. Rev.* **2017**, *46*, 5771-5804.

[6] a) G. Süss-Fink, *Dalton Trans.* **2010**, *39*, 1673-1688; J. Kljun and I. Turel, *Eur. J. Inorg. Chem.* **2017**, 1655-1666; b) J. Kljun, I. E. Leon, S. Peršič, J. F. Cadavid-Vargas, S. B. Etcheverry, W. He, Y. Bai and I. Turel, *J. Inorg. Biochem.* **2018**, *186*, 187-196.

[7] a) R. Hudej, J. Kljun, W. Kandioller, U. Repnik, B. Turk, C. G. Hartinger, B. K. Keppler, D. Miklavcic and I. Turel, *Organometallics* **2012**, *31*, 5867-5874; b) M. Schmidlehner, L. S. Flocke, A. Roller, M. Hejl, M. A. Jakupec, W. Kandioller and B. K. Keppler, *Dalton Trans.* **2016**, *45*, 724-733; c) W. Kandioller, C. G. Hartinger, A. A. Nazarov, M. L. Kuznetsov, R. O. John, C. Bartel, M. A. Jakupec, V. B. Arion and B. K. Keppler, *Organometallics* **2009**, *28*, 4249-4251.

[8] E. Shaw, J. Bernstein, K. Losee and W. A. Lott, *J. Am. Chem. Soc.* **1950**, *72*, 4362-4364.

[9] R. A. Jones and A. R. Katritzky, *J. Chem. Soc.* **1960**, *0*, 2937-2942.

[10] A. Bond and W. Jones, *Acta Crystallogr. C* **1999**, *55*, 1536-1538.

[11] N. L. Reeder, J. Kaplan, J. Xu, R. S. Youngquist, J. Wallace, P. Hu, K. D. Juhlin, J. R. Schwartz, R. A. Grant, A. Fieno, S. Nemeth, T. Reichling, J. P. Tiesman, T. Mills, M. Steinke, S. L. Wang and C. W. Saunders, *Antimicrob. Agents Chemother.* **2011**, *55*, 5753-5760.

[12] I. Machado, L. B. Marino, B. Demoro, G. A. Echeverria, O. E. Piro, C. Q. F. Leite, F. R. Pavan and D. Gambino, *Eur. J. Med. Chem.* **2014**, *87*, 267-273.

[13] E. R. Arce, M. F. Mosquillo, L. Perez-Diaz, G. A. Echeverria, O. E. Piro, A. Merlino, E. L. Coitiño, C. Maringolo Ribeiro, C. Q. F. Leite, F. R. Pavan, L. Otero and D. Gambino, *Dalton Trans.* **2015**, *44*, 14453-14464.

[14] a) H. Sakurai, H. Sano, T. Takino and H. Yasui, *Chem. Lett.* **1999**, *28*, 913-914; b) S. Takeshita, I. Kawamura, T. Yasuno, C. Kimura, T. Yamamoto, J. Seki, A. Tamura, H. Sakurai and T. Goto, *J. Inorg. Biochem.* **2001**, *85*, 179-186.

[15] C. Zhao, X. Chen, D. Zang, X. Lan, S. Liao, C. Yang, P. Zhang, J. Wu, X. Li, N. Liu, Y. Liao, H. Huang, X. Shi, L. Jiang, X. Liu, Z. He, Q. P. Dou, X. Wang and J. Liu, *Oncogene* **2016**, *35*, 5916-5927.

[16] C. Ma, J. Zhang and R. Zhang, *Can. J. Chem.* **2003**, *81*, 1070-1075.

[17] I. R. Baird, R. Mosi, M. Olsen, B. R. Cameron, S. P. Fricker and R. T. Skerlj, *Inorg. Chim. Acta* **2006**, *359*, 2736-2750.

[18] J. Kljun, M. Anko, K. Traven, M. Sinreih, Ž. Ude, E. E. Codina, J. Stojan, T. Lanišnik Rižner and I. Turel, *Dalton Trans.* **2016**, *45*, 11791-11800.

[19] a) W. Kandioller, A. Kurzwernhart, M. Hanif, S. M. Meier, H. Henke, B. K. Keppler and C. G. Hartinger, *J. Organomet. Chem.* **2011**, *696*, 999-1010; b) E. A. Enyedy, E. Sija, T. Jakusch, C. G. Hartinger, W. Kandioller, B. K. Keppler and T. Kiss, *J. Inorg. Biochem.* **2013**, *127*, 161-168.

[20] S. Ristovski, M. Uzelac, J. Kljun, T. Lipec, M. Uršič, Š. Zemljič Jokhadar, M. C. Žužek, T. Trobec, R. Frangež, K. Sepčić and I. Turel, *ChemMedChem* **2018**, *13*, 2166-2176.

[21] D. P. Martin, P. G. Blachly, J. A. McCammon and S. M. Cohen, *J. Med. Chem.* **2014**, *57*, 7126-7135.

[22] R. N. Adamek, C. V. Credille, B. L. Dick and S. M. Cohen, *J. Biol. Inorg. Chem.* **2018**, *23*, 1129-1138.

[23] F. Wang, A. Habtemariam, E. P. L. van der Geer, R. Fernandez, M. Melchart, R. J. Deeth, R. Aird, S. Guichard, F. P. A. Fabbiani, P. Lozano-Casal, I. D. H. Oswald, D. I. Jodrell, S. Parsons and P. J. Sadler, *Proc. Natl. Acad. Sci. U.S.A.* **2005**, *102*, 18269-18274.

[24] S. Seršen, J. Kljun, K. Kryeziu, R. Panchuk, B. Alte, W. Körner, P. Heffeter, W. Berger and I. Turel, *J. Med. Chem.* **2015**, *58*, 3984-3996.

[25] a) A. M. Pizarro, A. Habtemariam and P. J. Sadler in *Activation mechanisms for organometallic anticancer complexes, Vol. 32* (Eds.: G. Jaouen and N. Metzler-Nolte), Springer-Verlag, Berlin, **2010**, pp. 21-56; b) W. H. Ang, E. Daldini, C. Scolaro, R. Scopelliti, L. Juillerat-Jeannerat and P. J. Dyson, *Inorg. Chem.* **2006**, *45*, 9006-9013.

[26] T. S. Lobana and R. Singh, *Polyhedron* **1995**, *14*, 907-912.

[27] A. E. Egger, C. G. Hartinger, A. K. Renfrew and P. J. Dyson, *J. Biol. Inorg. Chem.* **2010**, *15*, 919-927.

[28] C. J. Sherr and J. Bartek, *Annu. Rev. Cancer Biol.* **2017**, *1*, 41-57.

[29] R. G. Kenny and C. J. Marmion, *Chem. Rev.* **2019**, *119*, 1058-1137.

[30] I. Romero-Canelon and P. J. Sadler, *Inorg. Chem.* **2013**, *52*, 12276-12291.

[31] a) J. J. Soldevila-Barreda, I. Romero-Canelon, A. Habtemariam and P. J. Sadler, *Nat. Commun.* **2015**, *6*, 9; a) S. J. Dougan, A. Habtemariam, S. E. McHale, S. Parsons and P. J. Sadler, *Proc. Natl. Acad. Sci. U.S.A.* **2008**, *105*, 11628-11633.

[32] W. Davis, Z. Ronai and K. D. Tew, *J. Pharmacol. Exp. Ther.* **2001**, *296*, 1-6.

[33] R. E. Carraway and P. R. Dobner, *Biochim. Biophys. Acta, Mol. Cell Res.* **2012**, *1823*, 544-557.

[34] F. Yang, Y. Zhang and H. Liang, *Int. J. Mol. Sci.* **2014**, *15*, 3580-3595.

[35] R. R. Ramsay, M. R. Popovic-Nikolic, K. Nikolic, E. Uliassi and M. L. Bolognesi, *Clin. Transl. Med.* **2018**, *7*, 14.

[36] X. Zhang, J. Lu, X. Ren, Y. Du, Y. Zheng, P. V. Ioannou and A. Holmgren, *Free Radic. Biol. Med.* **2015**, *89*, 192-200.

[37] Y. Ouyang, Y. Peng, J. Li, A. Holmgren and J. Lu, *Metallomics* **2018**, *10*, 218-228.

[38] P. Mura, M. Camalli, A. Bindoli, F. Sorrentino, A. Casini, C. Gabbiani, M. Corsini, P. Zanello, M. P. Rigobello and L. Messori, *J. Med. Chem.* **2007**, *50*, 5871-5874.

[39] L. Oehninger, M. Stefanopoulou, H. Alborzinia, J. Schur, S. Ludewig, K. Namikawa, A. Muñoz-Castro, R. W. Köster, K. Baumann, S. Wölfl, W. S. Sheldrick and I. Ott, *Dalton Trans.* **2013**, *42*, 1657-1666.

[40] N. Y. S. Lam, D. Truong, H. Burmeister, M. V. Babak, H. U. Holtkamp, S. Movassaghi, D. M. Ayine-Tora, A. Zafar, M. Kubanik, L. Oehninger, T. Söhnel, J. Reynisson, S. M. F. Jamieson, C. Gaiddon, I. Ott and C. G. Hartinger, *Inorg. Chem.* **2018**, *57*, 14427-14434.

[41] A. Casini, C. Gabbiani, F. Sorrentino, M. P. Rigobello, A. Bindoli, T. J. Geldbach, A. Marrone, N. Re, C. G. Hartinger, P. J. Dyson and L. Messori, *J. Med. Chem.* **2008**, *51*, 6773-6781.

[42] L. Oehninger, H. Alborzinia, S. Ludewig, K. Baumann, S. Wölfl and I. Ott, *ChemMedChem* **2011**, *6*, 2142-2145.

[43] Z. Luo, L. Yu, F. Yang, Z. Zhao, B. Yu, H. Lai, K. H. Wong, S. M. Ngai, W. Zheng and T. Chen, *Metallomics* **2014**, *6*, 1480-1490.

[44] C. Schmidt, B. Karge, R. Misgeld, A. Prokop, R. Franke, M. Bronstrup and I. Ott, *Chem. Eur. J.* **2017**, *23*, 1869-1880.

[45] D. J. Daigle, T. J. Decuir, J. B. Robertson and D. J. Darensbourg in *1,3,5-Triaz-7-phosphatricyclo[3.3.1.1^{3,7}]decane and derivatives, Vol. 32* (Ed. M. Y. Darensbourg), John Wiley & Sons, Inc., Hoboken, New Jersey, USA, **1998**, pp. 40-45.

[46] O. V. Dolomanov, L. J. Bourhis, R. J. Gildea, J. A. K. Howard and H. Puschmann, *J. Appl. Crystallogr.* **2009**, *42*, 339-341.

[47] G. Sheldrick, *Acta Crystallogr. A* **2015**, *71*, 3-8.

[48] A. Bolje and J. Košmrlj, *Org. Lett.* **2013**, *15*, 5084-5087.

[49] A. Jankowiak and P. Kaszynski, *J. Org. Chem.* **2009**, *74*, 7441-7448.

[50] J. Skiba, C. Schmidt, P. Lippmann, P. Ensslen, H. A. Wagenknecht, R. Czerwieniec, F. Brandl, I. Ott, T. Bernas, B. Krawczyk, D. Szczukocki and K. Kowalski, *Eur. J. Inorg. Chem.* **2017**, 297-305.

Table of Content

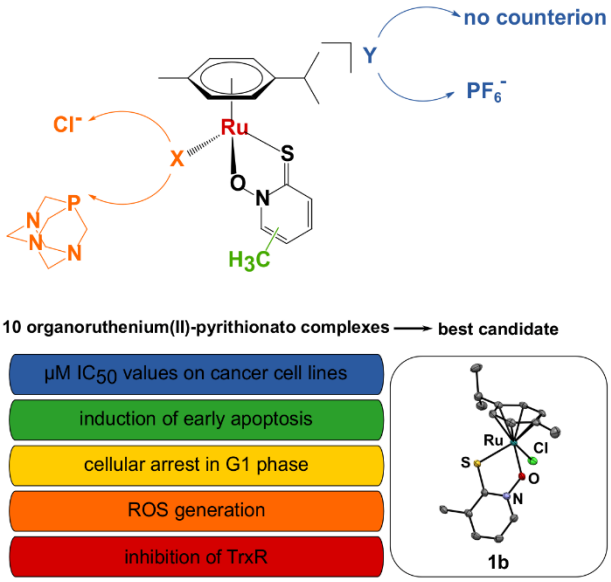

The first extended study of organoruthenium(II)-pyrithionato compounds to explore the influence of minor structural alterations on anticancer activity. To obtain full potential of these compounds organic thiohydroxamic ligand must be bound to ruthenium scaffold with labile chloride to achieve all desired anticancer properties.